Study of Acidic and Basic Properties of Silica-Magnesia Catalysts in the Conversion of Ethanol into 1,3-Butadiene

Master Research Thesis by Marjolein E.Z. Velthoen Bsc.
Supervisors: Carlo Angelici Msc.
Dr. Pieter C.A. Bruijnincx
Prof. Dr. Bert M. Weckhuysen
Department of Inorganic Chemistry and Catalysis
Debye Institute Utrecht University
January 2014

Abstract

The Lebedev process, in which ethanol is converted into 1,3-butadiene, proceeds through multiple elementary steps, either acid- or base catalyzed. The acidic and basic properties of catalysts are thus related to the catalytic performance; in particular, a high amount of ethylene production indicates a high concentration of accessible acidic sites present in the catalyst. In this thesis, the acidic and basic properties of differently prepared silica-magnesia catalysts, used in the Lebedev process, were studied with both bulk- and spatially-resolved characterization techniques. Furthermore, the influence of doping the silica-magnesia catalysts with small dispersed CuO particles on the acidic and basic properties was studied.

All catalysts contained silica and magnesia in equimolar ratios and were prepared via either a co-precipitation route (CP and CP-MOD) or via wet-kneading employing different silica sources (WK, WK-MOD, WK-AER and WK-BIG). A second series of these catalysts was promoted with 1 wt% CuO using incipient wetness impregnation.

NH_3-TPD showed that the CP catalyst contained the highest concentration of acidic sites and the WK catalyst the lowest. The CP-MOD, WK-MOD and WK-AER showed similar concentrations of acidic sites. Upon CuO promotion, the concentration of acidic sites decreased for all samples, except for the WK-AER catalyst, for which it increased significantly. Pyridine-FTIR showed that CP contained the highest concentration of acidic sites and WK the lowest, which is consistent with the results from NH_3-TPD. Moreover, pyridine-FTIR showed that the strongest acidic sites are present in the CP catalyst and the weakest in the CP-MOD. Spectra of CuO-promoted catalysts showed that CuO particles are anchored to the surface hydroxyl groups, with a preference for the hydroxyl groups on the magnesia moiety. Upon CuO-promotion, it was shown that the concentration of acidic sites decreased significantly for the co-precipitated samples and slightly for the wet-kneaded catalysts; this is not in line with NH_3-TPD, which showed an increase for WK-AER. Pyridine-FTIR showed that WK lost all acidic sites upon CuO-promotion. The acidic sites in CP and CP-MOD became weaker, shown by a lower desorption temperature, whereas the WK-MOD and the WK-AER catalysts became stronger upon CuO-doping, shown by a higher desorption temperature.

A study employing Hammett indicators showed that WK contained the strongest basic sites and CP the weakest. Deuterated chloroform-FTIR showed that all catalysts contained weak and strong basic sites, with WK containing the strongest and CP the weakest. Moreover, it was shown that magnesia only contains weak basic sites, which is inconsistent with the results from the Hammett indicator study, showing the presence of strong basic sites in magnesia. Upon CuO-promotion, the CP catalyst shows a considerable decrease in concentration of basic sites. For the WK catalyst, CuO-promotion considerably influences the strength of the basic sites. Promotion with CuO does not cause a significant variation in the basic properties of the WK-MOD catalyst.

Content

Chapter 1. Introduction

In the last decades, the depletion of fossil fuels has been recognized as inevitable in the coming future. This awareness brings up the need to explore alternative resources. Nowadays, society depends on the supply of fossil fuels, such as gas, oil and coal, for both the world energy provision and chemical production. However, since the fossil fuel resources are running down, alternative supplies must be explored to fulfill the need for energy and chemical production. In order to find these alternative resources to replace fossil fuels, extensive research is required.[1]

In addition to economic reasons, the current environmental problems, caused by the emissions of harmful greenhouse gases connected with the use of fossil fuels, also encourage to find alternatives for fossil fuel resources. In the recent years, society has gained increasing interest into finding solutions for the current environmental problems. The possible replacement of fossil fuel resources by renewable ones could lead to a significant reduction of emitted greenhouse gases.[2] Possible alternative renewable resources include photo-synthetic, wind-based, geothermal and biomass-based resources.[3] Whereas the previous listed resources can all be explored for energy supply, biomass-derived feedstocks are considered the best candidates for the production of bulk chemicals.[4,5] Biomass is biological material derived from (recently) living organisms. It also often refers to plant-derived materials.[6] Biomass can be found anywhere around the world, regardless of climatic conditions. However, to serve as a substrate for the production of bulk chemicals, non-edible lignocellulosic biomass is preferred, since this biomass component does not suffer from interference with the food industry.[7]

The use of biomass as a renewable resource has several important advantages. First of all, its use could decrease the reliance of chemical industry on non-renewable resources; moreover, the development of biomass-based processes would be beneficial from an economic and environmental point of view, given that biomass-derived chemicals are reported to be CO_2-neutral.[3,8].

Research into the synthesis of biomass-derived value-added chemicals is multidisciplinary and involves different aspects such as optimization of catalysts or reaction conditions.[5,9,10] Nowadays, many research groups worldwide investigate diverse possibilities for the exploitation of biomass.[4,7,11] Ethanol is an example of which nowadays already 90% of its production is biomass-derived.[12] The main application (67%) of bioethanol is its use as biofuel, however, once production volume increases, it is expected that the prices will decrease significantly. This could make bioethanol an interesting platform-molecule in the production of bulk chemicals, e.g. butadiene.[3] Butadiene is a high-value platform molecule with large applications in the polymer industry. Currently, 95% of all produced butadiene is obtained as a byproduct in the production of ethylene by steam cracking. However, resources, such as natural gas or shale gas, are being explored as an alternative for oil, which is expected to lead to a decrease in butadiene production. Therefore, new routes towards the production of butadiene need to be investigated.[13]

This master thesis concerns the use of bio-ethanol as renewable feedstock in the production of 1,3-butadiene (referred to herein as butadiene) and in particular the study of the acidic and basic properties of the catalysts employed in this reaction.

1.1 Bioethanol

Ethanol can be produced via the petrochemical route and from biomass. Nowadays, 90% of all ethanol produced is biomass-derived, which is mainly applied as a biofuel. Since oil prices are constantly increasing, the petrochemical route becomes progressively less attractive and large-scale research is done on high-volume ethanol production from biomass in order to not only use it as a biofuel, but also as a feedstock in the production of bulk chemicals.[12,14]

Bioethanol is the term for ethanol, produced from plants. It is considered one of the most promising bio-based chemicals, mainly because of its potentially high-volume production and because it is both a renewable and versatile platform-molecule.[3] Over the past decades, the production of bioethanol (expected to reach 105 billion liters in 2016 [15]) increased significantly (see Figure 1). A direct consequence of this considerably growing production is the expected decrease in price (700 €ton^{-1} in November 2012 on the European market[16]). This makes bioethanol a very promising bio-derived chemical.
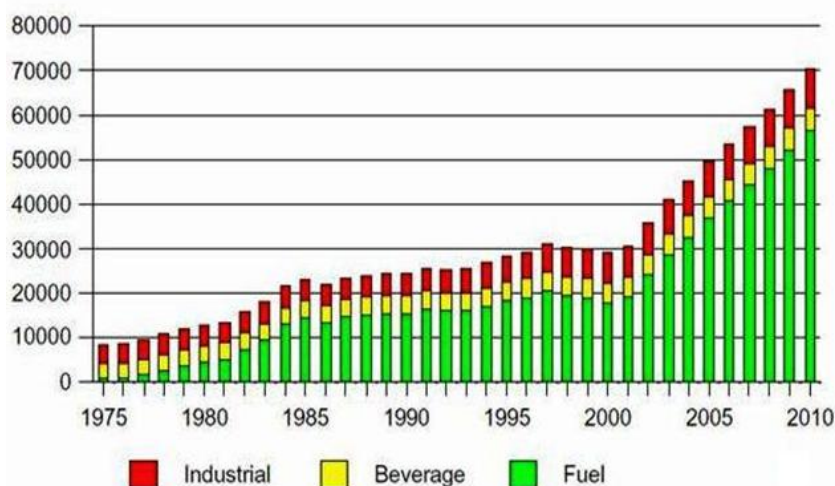

Figure 1: Worldwide production of ethanol over the period 1975-2010[17]

The conventional pathway for the production of bioethanol is the fermentation of sugars. Unfortunately, this so-called 1st generation bioethanol production suffers from competition with the food industry, as sugars are mainly explored for food production.[10,18] Because of this, other renewable resources, such as non-edible biomass feedstocks, are preferred to 1st generation bioethanol.[11,19] Examples are 2nd generation- (conversion of non-fermentable sugars or lignocellulosic fraction of biomass)[20,21] and 3rd generation processes (conversion of algae and seaweeds) for the production of ethanol.[22,23]

Nowadays, 90% of the ethanol on the market is biomass-derived.[12] The main application of bioethanol is its use as a biofuel (67%). An additional increase in production volume followed by a predictable decrease in its market prices would make an extensive use of bioethanol for the production of high-value bulk chemicals economically more beneficial.[3]

1.2 Butadiene

Butadiene is a high-value platform molecule with large applications in the polymer industry. More than 50% of the use of butadiene is covered by the production of polybutadiene and styrene-butadiene rubber (SBR), used in car tire production.[24] Currently, 95% of all produced butadiene is obtained as a byproduct in the production of ethylene by steam cracking. The downside of this process is the high number of separation steps required to obtain butadiene of commercial purity.[13] Also, the significant increase in oil prices, together with the availability of lighter feedstocks (also due to the renowned shale gas boom) for the cracking processes involved in the production of ethylene threaten butadiene production and are expected to eventually lead to an increase in its market price.[3] Therefore it is important to explore alternative processes for the production of butadiene.

1.3 Lebedev Reaction

In the beginning of the twentieth century, Ostromislenskiy found a two-step process to obtain butadiene from ethanol, in which ethanol is first dehydrogenated to form acetaldehyde, followed by reaction with an additional ethanol molecule to yield butadiene, catalyzed by a metal-oxide.[25] A few decades later, Lebedev showed that it is possible to produce butadiene from ethanol in one step over a bifunctional catalyst, with both dehydrating and dehydrogenating activity. This reaction is shown in Scheme 1.[26-28] The catalyst for the Lebedev process was reported to consist of a mixture of silicon and magnesium oxides with small amounts of other oxides as promoters.[29] Although the one-pot Lebedev process is generally reported to result in lower butadiene yields and purities as obtained by the two-step Ostromislenskiy process, the latter is experimentally more complicated and expensive. For these reasons, the Lebedev process is industrially highly desirable and therefore favored over the two-step Ostromislenskiy process when applied to large scale butadiene production. In order to apply the Lebedev process on industrial scale, research is done to further optimize the process.[3]
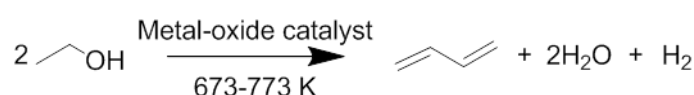
Scheme 1: The overall reaction for the one-step Lebedev process for the production of butadiene from ethanol

1.3.1 Mechanism

The mechanism of the conversion of ethanol into butadiene according to the one-pot Lebedev process is still debated. It is generally accepted that the formation of butadiene from ethanol involves several elementary steps. The mechanism proposed by Toussaint and co-workers for the Lebedev process is widely accepted, although no definite proofs have so far been reported. The proposed mechanism is based on the aldol condensation between two acetaldehyde molecules, as can be seen in Scheme 2.[30]
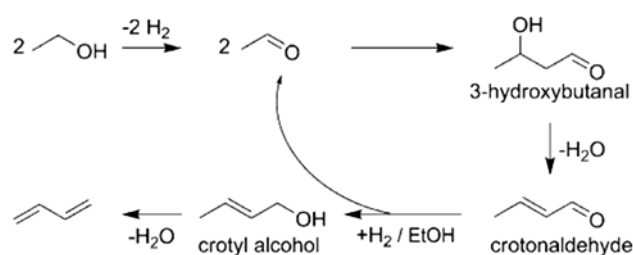
Scheme 2: The aldol condensation mechanism as proposed by Toussaint et al.[30]

Acetaldehyde is formed upon ethanol dehydrogenation and 3-hydroxybutanal is generated after aldol condensation, dehydration of the latter leads to crotonaldehyde formation. Finally, crotonaldehyde is hydrogenated and then dehydrated leading to the desired product butadiene. Each elementary step as described above is catalyzed by the presence of either acidic or basic sites. Ethanol dehydrogenation is catalyzed by (the presence of) basic sites. The formation of 3-hydroxybutanal can either be catalyzed by acidic or basic sites and the consequent dehydration takes place on acidic sites. Subsequent hydrogenation requires basic active sites and the final dehydration step, leading to the formation of the desired product butadiene, demands the presence of acidic sites again. An efficient conversion of ethanol into 1,3-butadiene therefore requires a balanced ratio between accessible acidic and basic sites to prevent the formation of an excess of intermediate products.

An alternative mechanism for the formation of butadiene from ethanol was proposed by Fripiat *et al.*[31] The suggested mechanism involves a Prins-like condensation between ethylene and acetaldehyde, the former being formed by dehydration of ethanol on acidic sites and the latter being formed by dehydrogenation of ethanol on basic sites. The condensation reaction, catalyzed by acidic active sites, between ethylene and acetaldehyde yields but-3-en-2-ol, which is dehydrated to finally produce butadiene, as showed in Scheme 3.[31]
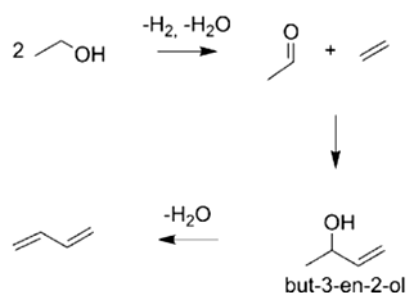
Scheme 3: The Prins condensation mechanism as proposed by Fripiat et al [31]*.*

Fripiat *et al.* confirmed the importance of acetaldehyde production as an intermediate for butadiene formation, but also pointed out at the involvement of ethylene (by dehydration of ethanol) as a key intermediate. The two proposed mechanisms show that the catalysts in the Lebedev synthesis are required to have a certain degree of both acidity and basicity as each elementary step is either acid- or base catalyzed. However, if the degree of acidity is too high, large amounts of dehydration by-products like ethylene are produced. For this reason, the amount of ethylene produced can be used as an indirect indication of the amount of acidic sites in the catalyst. Moreover, if the degree of basicity is significantly prevailing over the acidic properties, large amounts of (de)hydrogenation by-products, such as acetaldehyde, are produced. Therefore, as mentioned before, catalysts employed in the Lebedev synthesis, are required to possess an optimal ratio of acidic and basic properties. This master thesis focuses on the study of the acidic and basic properties of the catalysts used in the Lebedev process, in order to relate the results herein reported to the catalytic performances and to the proposed mechanism.

1.3.2 Catalytic System

The composition of the catalyst developed by Lebedev to convert ethanol into butadiene has been the topic of research for decades. Around 1945, Natta and Rigamonti reported to have found its composition and claimed that the catalyst consisted of both silica and magnesia.[32,33]

A few decades later, Niiyama and co-workers studied different catalytic silica-magnesia systems. They reported that an increase in magnesia content significantly improves catalytic activity, but magnesium oxide alone shows no activity. The optimum amount of MgO was reported to be 85%, which showed that a small amount of silica notably increases the activity and selectivity towards butadiene.[34]

Afterwards, various researchers showed that different methods for catalyst preparation considerably influence catalytic activity in the Lebedev process. The activity of catalysts, which were prepared by kneading silica and magnesium hydroxide in water, was compared with the activity of catalysts co-precipitated from magnesium chloride and tetraethyl orthosilicate (TEOS). The former catalysts showed higher activity.[35] Kvisle *et al.* also showed that a chemical mixture of equimolar quantities of silica and magnesia (prepared via wet-kneading), leads to higher catalytic activity and stability in the Lebedev process as compared with physically mixed catalysts in equimolar ratios, thus highlighting a synergistic effect between the two oxides.[36]

Introduction

Recently, the influence of doping silica-magnesia systems with different transition metal oxides such as chromium, iron, cobalt, nickel, copper or zinc on the catalyst performance was reported. It was demonstrated that doping with these transition metal oxides improves butadiene selectivity and activity and, at the same time, lowers ethylene selectivity.[37] Makshina *et al.* showed that for SiO_2-MgO systems, employed in the Lebedev synthesis, doping with transition metal oxides, significantly improved butadiene yield and selectivity. These improved results, indicating the achievement of a more beneficial ratio between acidic and basic sites, were especially achieved by doping the catalysts with copper(II)oxide and zinc oxide. Copper(II)oxide showed an increase in butadiene yield by a factor of 4 compared with the non-promoted SiO_2-MgO catalysts and an increase in butadiene selectivity by a factor of 1.5. Zinc oxide showed a similar increase in butadiene selectivity and an increase in butadiene yield by a factor of 3 compared with the non-promoted catalysts. Together with this increase in activity towards butadiene, the ethylene production was decreased upon promotion with transition metal oxides.[29]

The studied catalysts in this master thesis all consist of equimolar ratios of silica and magnesia and were prepared with different methods to study the influence of preparation method on the acidic and basic properties of the catalysts. Since the wet-kneading procedure was reported to have a positive impact on the catalytic performance ([35,36]), the acid/base properties of wet-kneaded catalysts were studied and compared with co-precipitated catalysts. Furthermore, the influence of CuO-promotion on the acidic and basic properties was investigated in order to relate these results to the improved catalytic performances.

1.3.3 Previous Work

Previous work in this group has been done on the catalytic performance of five differently prepared silica-magnesia systems as catalysts in the Lebedev reaction. Three catalysts were prepared following a wet-kneading procedure similar to what was reported by Kvisle *et al.*[36], employing magnesium hydroxide and silica spheres (prepared following a Stöber-like approach [38]) with different particle sizes. The catalysts, hereafter referred to as **WK**, **WK-MOD** and **WK-AER**, employed respectively relatively large silica spheres (≈ 425 nm), smaller spheres (30-100 nm) and commercial Aerosil 300 silica (20-40 nm), as purchased by Degussa. Two catalysts were prepared by using a co-precipitation method, similar to what was described by Brambila *et al.*[39] The **CP** catalyst was prepared by co-precipitating the silica- and magnesia precursors in an ammonia/ethanol mixture. The last catalyst, referred to as **CP-MOD**, was also prepared by co-precipitation, but first silica spheres were allowed to form for 20 minutes before addition of the magnesia precursor solution.

Improved catalytic performances were achieved when doping the silica-magnesia systems with copper(II)oxide. Therefore, the previously described silica-magnesia systems were impregnated with 1 wt% copper oxide, (similar to what was described by Makshina *et al.*[29]) yielding five new catalysts, called **CuO/WK**, **CuO/WK-MOD**, **CuO/WK-AER**, **CuO/CP** and **CuO/CP-MOD**.

In total, ten catalysts were prepared and their catalytic performance was tested (see Figure 2). The left part of the figure shows catalytic performances of the SiO_2-MgO systems, whereas the right part shows this for the CuO-promoted SiO_2-MgO catalysts. The figure shows that copper(II)oxide-doping indeed has a promoting effect on the butadiene production. The left graph in Figure 2 shows that, although the catalysts contain silica and magnesia in the same molar ratio of 1:1, their catalytic performances differ significantly. The wet-kneaded catalysts lead to higher butadiene and lower ethylene yields than the co-precipitated ones. To explain these differences in catalytic performances, it is proposed that different preparation methods lead to differences in the acid-base properties of the various catalysts. The proposed mechanisms for the Lebedev synthesis, as described in section 1.3.1, support this hypothesis, because the different acid/base-catalyzed elementary steps suggest that varying the ratio between acidic and basic sites influences the product distribution during catalytic performance. For instance, high yield of ethylene is an indication of a high concentration of (accessible) acidic sites.
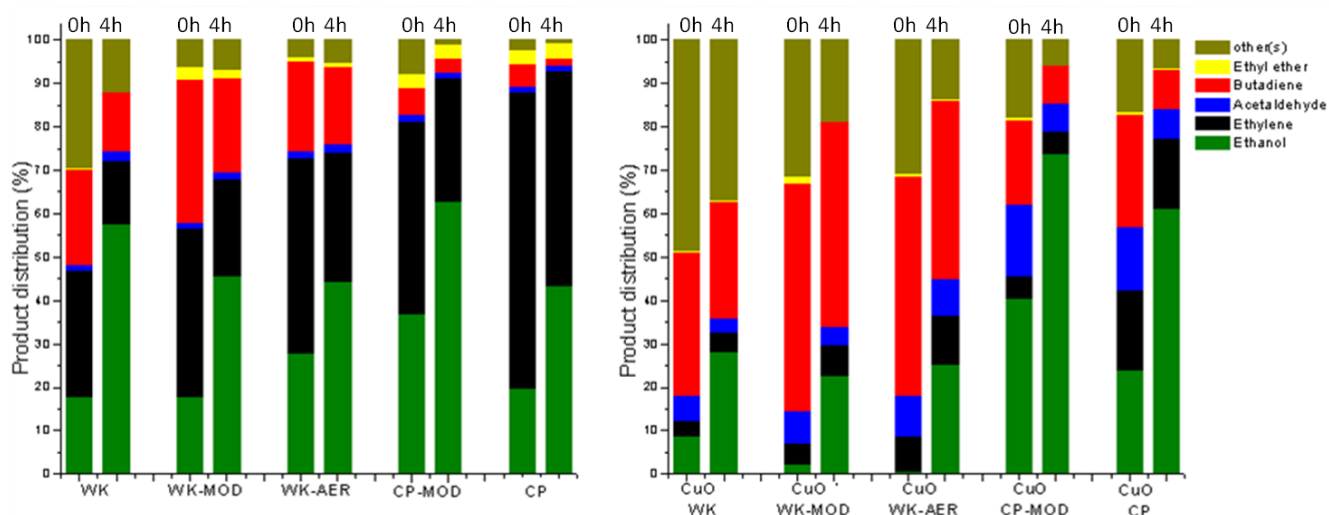
Figure 2: Catalytic performances of the catalysts employed in the Lebedev reaction. SiO$_2$-MgO catalysts are reported on the left, the same catalysts doped with CuO are on the right. In each graph, the bars on the left indicate the initial result (0h), whereas those on the right indicate results after 4h.

In Figure 3, the TEM micrographs of the five SiO$_2$-MgO catalysts (WK, WK-MOD, WK-AER, CP and CP-MOD) are reported; differences in morphology can be indirectly related with differences in amount and strength of the active sites in the catalysts. In WK, the two components (silica and magnesia) can be clearly distinguished and the silica spheres appear to be embedded in a thin magnesium oxide layer. The same characteristics can be observed in WK-MOD (in this catalyst, silica spheres are smaller in size). Both catalysts have silica-rich and magnesia-rich areas. In WK-AER, the two components can still be recognized, but no silica-rich areas could be identified. The quite small silica spheres (in the range 20-40 nm) are embedded in magnesia. The two co-precipitated samples differ significantly from each other in morphology. It can be observed that in CP-MOD the silica spheres are covered in magnesia layers, which do not have the platelet-like structure anymore, as is the case in the WK catalyst. Whereas in CP-MOD the two components can be clearly distinguished, the CP catalyst has an ill-defined morphology. In the latter, silica spheres or magnesia platelets could not be identified as in the other catalysts.
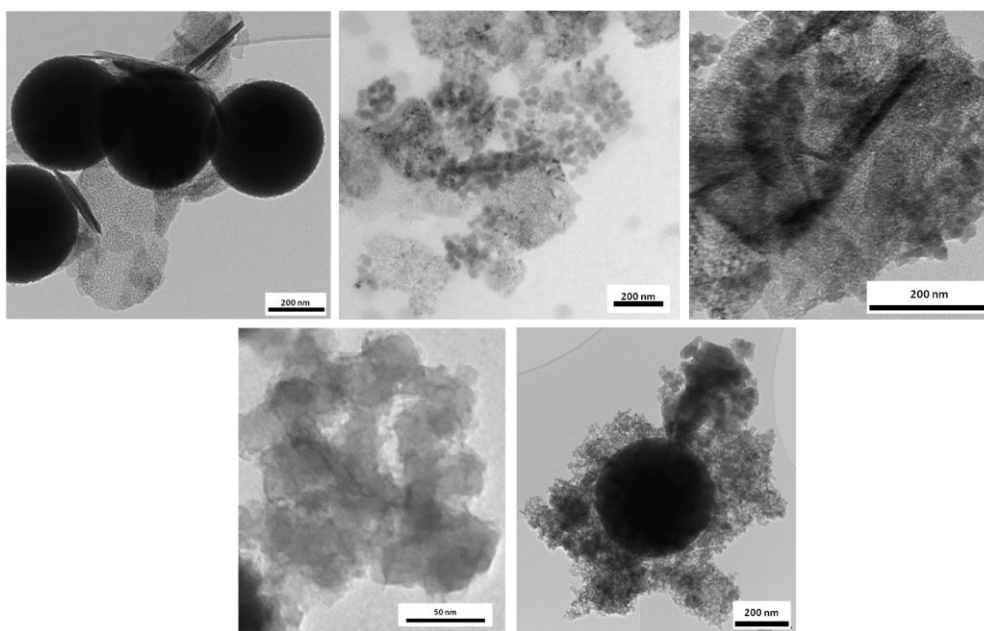
Figure 3: TEM micrographs showing the morphology of wet-kneaded catalysts, from left to right (top): WK, WK-MOD and WK-AER and co-precipitated catalysts: from left to right (down): CP and CP-MOD

1.4 Aim and Approach

The aim of this thesis is to study acidic and basic properties of the ten catalysts described above and to explain the influence of preparation method and CuO-doping on acid-base properties and catalytic performance of these catalysts with the use of both bulk- and spatially-resolved techniques. Bulk characterization techniques give averaged values of the acid-base properties of the studied catalysts and give an indication about the overall acidity/basicity of the catalysts. Spatially-resolved characterization techniques are employed to study the acidic and basic properties of the catalyst at a local level and can be employed to determine the actual location and nature of acidic and basic active sites.

The employed bulk techniques were ammonia-Temperature Programmed Desorption (NH_3-TPD), Hammett indicators, pyridine- and deuterated chloroform-Fourier Transform Infrared Spectroscopy (FTIR) and the spatially-resolved technique used is Coherent Anti-Stokes Raman Scattering (CARS).

Chapter 2. Theory

2.1 Catalyst Preparation

In this thesis, different methods were employed to prepare the catalysts and study the effect of preparation on the catalytic performances and the related acidic and basic properties.

1. SiO_2 preparation
2. $Mg(OH)_2$ preparation
3. Wet-kneading
4. Co-precipitation
5. Incipient wetness impregnation

2.1.1 Stöber-SiO$_2$ Preparation

Silica can be prepared using a sol-gel synthetic method in which the silica precursor is first hydrolyzed and subsequently polymerized to form silica having a spherical morphology (i.e. Stöber-like silica).[38]The process for preparing silica spheres in one batch involves a hydrolysable silica precursor, an alcohol, ammonia and water; depending on the nature of the alcohol and proportion of the different chemicals, two phases can be formed. In this case, one phase consists of the silica precursor, preferably a tetraalkoxysilane, such as tetraethoxysilane. The second phase is an aqueous ammonia solution. An alcohol can be present in one or both phases. At least one of the two phases must contain an alcohol. Any alcohol can be employed, but typically the selected alkanol is the same as the alkanol generated via hydrolysis of the employed tetraalkoxysilane. Silica is formed by hydrolysis of the tetraalkoxysilane due to the presence of ammonia and water. In this process, an alkanol molecule is formed as a side-product. As hydrolysis takes place, the two phases, whether present, merge into one. In the two-phase solution, the microspheres can grow, thus to increase the time during which two distinct phases are present, the composition of the reacting solutions has to be adjusted, for instance by adding the tetraalkoxysilane in small separate batches.[38]

There is a number of parameters which can be adjusted to vary the (average) size of the silica spheres, prepared in this method. First of all, the choice of the tetraalkoxysilane and corresponding alkanol can be influential. An increase in the length of the carbon-chain, leads to an increase in the average size of the resulting silica spheres. There is, however, a tendency toward wider size distributions when using tetraalkoxysilanes with longer carbon chains.[38,40] Furthermore, concentrations and overall conditions in the feed solutions also influence the result for average size, e.g. low reaction temperatures and higher ammonia concentration, lead to larger particles. A concentration of water around 8 mol/dm^3 favors the formation of the largest particles.[40,41]

2.1.1.1 Nucleation and Growth

When preparing silica spheres, ammonia is usually added to the phase containing the silica precursor. However, in order to prepare (relatively) small silica spheres, the silica precursor should be added to the ammonia phase, thus favoring the nucleation step over particle growth.[42,43]

2.1.1.2 Synthesis of Large Silica Spheres

For the study of a SiO_2-MgO system with Coherent Anti-stokes Raman Scattering (CARS), the system needs to contain silica spheres with sizes larger than 425 nm (employed in WK) in order to surpass the diffraction limit. Many papers have been published on the synthesis of monodisperse silica spheres with diameters larger than 500 nm.[38,40,41,43-45] In these publications, two different methods are commonly employed; the first involves the preparation of silica spheres in one batch, while in the second method spheres are grown from a seed solution, a suspension of silica spheres prepared as described in section 2.1.1.[44]

In the second method to synthesize larger spheres, the silica spheres are allowed to grow from a seed solution. In the first step, the seed solution is prepared according to the method described

above. Next, two solutions (the tetraalkoxysilane- and the ammonia solution) are fed slowly and continuously to the seed solution under uniform mixing. This continuous addition is usually performed at a controlled rate in order to only react with the silica particles present in the solution. This rate should be adjusted to prevent the presence of an excessive amount of tetraalkoxysilane in the solution, thus leading to formation of new particles. The final particle size depends on the amount of tetraalkoxysilane added in total and on the initial particle size of the silica spheres in the seed solution.[43,45]

2.1.2 Mg(OH)$_2$ Precipitation

Magnesium hydroxide is formed when a base, e.g. ammonia, is added to a magnesium precursor. The magnesium ions from the magnesium precursor precipitate with the hydroxide ions, forming magnesium hydroxide.[35]

2.1.3 Wet-Kneading

The wet-kneading procedure was reported by Kvisle *et al*. and in their study it was used for the chemical mixing of silica spheres (prepared previously) and magnesium hydroxide in water for four hours at room temperature. The wet-kneading procedure is not commonly used in catalyst preparation, therefore not much is known about the theory behind this preparation method. It is assumed that, during reaction, hydrolysis can occur leading to the formation of chemical bonds between the two components.[36] In the considered study this would occur between hydroxyl groups present on the surface of silica and magnesium hydroxide.

2.1.4 Co-Precipitation

Co-precipitation is a technique in which a solid is precipitated from a solution containing two or more (metal) precursors. When preparing silica-magnesia systems with the co-precipitation technique, the two precursors Mg(NO$_3$)$_2$ and TEOS (tetraethyl orthosilicate) are precipitated at the same time in a basic environment in order to achieve structures such as M'-O-M'' (in the considered study, M' and M'' represent silicon and magnesium atoms). The basic character of the solvent catalyzes the hydrolysis and precipitation of both precursors.[39]

2.1.5 Incipient Wetness Impregnation

There are two types of impregnation; in wet impregnation an excessive amount of precursor solution is used, while in incipient wetness impregnation (also called dry impregnation) the amount of precursor solution equals the total pore volume of the porous support. During dry impregnation the porous support is impregnated to incipient wetness with a solution of the precursor. Due to capillary forces, the solution is pulled inside the support and the precursor is distributed over the support. The impregnation can be done with organic precursors since they have proven to provide a good dispersion. However the solubility of an organic precursor is generally very low, resulting a very low occupancy of the support's surface. As inorganic precursors have a high solubility in water they are preferred in the solution impregnation method. Metal nitrates are known for their high solubility in water and low waste production when used in incipient wetness impregnation and are therefore often used. The downside is that while metal nitrates allow for high loadings, the resulting dispersions are often very poor.[46]

2.2 Characterization Techniques

The acidic and basic properties of the prepared catalysts were studied as they are proposed to play a key-role in the catalytic conversion of ethanol into butadiene. Four characterization techniques were used in this project to determine the bulk acidity and basicity of the prepared catalysts.

1. Coherent Anti-Stokes Raman Scattering (CARS) Micro-Spectroscopy
2. Fourier Transform Infrared Spectroscopy (FTIR) with probe molecules
3. Ammonia-Temperature Programmed Desorption (NH$_3$-TPD)
4. Hammett Indicators

The last three techniques are defined bulk techniques, as they provide averaged information of the bulk material on the acidic and basic properties of the catalysts, regardless of microscopic differences inside the catalyst. Thus, these techniques do not provide any specific surface related information, but give an indication about the overall acidity/basicity of the catalysts. CARS, on the other hand, is a spatially-resolved technique, thus it allows the study of, e.g., the location of acidic and basic sites in the catalyst. Since Hammett indicators and CARS are not commonly employed procedures in characterization studies, the fundamentals of the techniques will be explained in this chapter. For the FTIR studies with probe molecules, more information will be given in this chapter on the assignment of the bands observed in the IR-spectra.

2.2.1 Coherent Anti-Stokes Raman Scattering (CARS) Micro-Spectroscopy

In Raman spectroscopy, the interaction between light and matter allows to study the chemical nature of the matter under investigation. Infrared and Raman spectroscopy are usually considered complementary techniques, because a bond vibration is IR active when there is a change in dipole moment during the vibration, while it is Raman active if the vibration causes a change in polarizability.[47] In Raman spectroscopy, monochromatic light, usually from a laser, interacts with molecular vibrations in the studied system. As a result, the energy of the scattered laser photons is shifted. This shift in energy gives information about the vibrational modes in the system.[48]

Coherent Anti-Stokes Raman Scattering is based on Raman spectroscopy, but it also combines microscopy to study local properties of the sample under investigation.[48,49] This combination of spectroscopy and microscopy makes CARS also an interesting method to apply in chemical imaging of biological processes.[50-52] Compared with Raman spectroscopy, CARS employs a large amount of photons to address the molecular vibrations, resulting into a coherent signal. This makes the CARS signal stronger than Raman. There exist two types of Raman scattering: the Stokes and the anti-Stokes scattering. In Stokes scattering, the studied material absorbs energy and emits a photon with a lower energy than the absorbed photon (transition of an electron from a low to a high energy state). The frequency of the Stokes scattering is in the same range as fluorescent signals. In anti-Stokes scattering, the material loses energy and the emitted photon possesses a higher energy than the absorbed photon (transition of an electron from a high to a low energy state). In Raman spectroscopy, the Stokes scattering is prevailing over the anti-Stokes signal.[47,53]

In CARS, two laser beam frequencies (one from the pump with a frequency ω_{pump} and one Stokes laser with a frequency similar to the Stokes signal ω_{stokes}) overlap in time and interact with the sample. Once a molecular vibration, present in the sample coincides with the frequency difference, the CARS signal at the anti-Stokes frequency is enhanced, leading to a coherent optical signal. The anti-Stokes signal is equal to $2\omega_{pump} - \omega_{stokes}$. Compared to Raman spectroscopy, where the signal is based on spontaneous Raman emission, the coherent CARS signal shows a signal with an intensity which is 10^6 stronger.[54] Another advantage of CARS is the use of the anti-Stokes signal, which does not interfere with fluorescent signals from the catalyst, leading to spectra characterized by lower noise.[53] The combination of CARS with microscopy (with a spatial resolution of 0.6 x 0.6 x 3.5 μm^3) allows to study the location of Raman-active molecules and, for example, allows the use of probe molecules, thus studying acidic and basic sites of a catalyst.[47,53]

2.2.2 Fourier Transform Infrared Spectroscopy (FTIR) of Adsorbed Probe Molecules

Interaction of infrared radiation with a mode of vibration only occurs when the electric field of radiation oscillates with same frequency as instant dipoles caused by atomic vibrations. A normal vibration is therefore IR active only if a change in the dipole moment of the vibration occurs and is a one photon process, as only photon is absorbed.[55] The use of probe molecules, due to the interaction of those with active sites in the sample of interest, allows the study of acidic and basic sites. A basic probe molecule, for example, can interact with an acid site of the studied sample, thus this interaction generates a new band or causes a shift in a known band of the probe molecule. In

this study, pyridine and deuterated chloroform were used to probe, respectively, the acidic and basic sites of the investigated catalysts.

2.2.2.1 Pyridine-FTIR

Pyridine-FTIR is commonly used to study the acidic properties of catalysts. Other commonly used probe molecules include CO, NH_3 and NO.[56] Pyridine is a basic molecule (pK_B = 8.75 [57]) and is often preferred to the other molecules, since it is more selective and less reactive than NH_3, it shows stronger adsorption on acidic surfaces than CO and it is relatively more sensitive to Lewis acidic sites than NO.[57-59] To achieve an accurate measure, in pyridine-FTIR, the catalyst surface has to be free from other adsorbed molecules (e.g. water and carbon dioxide); this is commonly achieved by heating up the catalyst under vacuum. IR-spectra can be taken during this process to observe the removal of those molecules which would hinder pyridine adsorption on the catalyst surface. In the OH-region (3500-3800 cm^{-1}) several peaks can be seen upon drying due to dissociative adsorption of residual H_2O molecules, forming hydroxyl groups on the surface.[59,60] Initially, a broad band can be observed due to the presence of H_2O molecules. However, temperature increase favors H_2O desorption, thus allowing the observation of one or more peaks due to hydroxyl groups present on the investigated materials. These peaks are characteristic of the nature of the surface hydroxyl groups. CO_2 adsorption on basic catalysts leads to the observation of two broad bands in the range 1400-1600 cm^{-1}, which decrease in intensity during the drying process due to the desorption of the CO_2 molecules. These bands are assigned to mono- and bidentate CO_2 adsorbed on solid materials.[61,62]

Once the adsorbed molecules have been removed, the probe molecule can be introduced in the spectroscopic cell where the catalyst has been placed. Pyridine adsorption on Lewis or Brønsted acid sites originates different peaks in IR analysis; the position of these peaks indicates the type of acidic sites and their intensities give an indication of the concentration of acidic sites present in the sample. A TPD program (Temperature-Programmed Desorption) can be used increasing the temperature of the cell containing pyridine adsorbed on the catalyst to study the strength of the acidic sites involved, as pyridine adsorbed on weak acidic sites will be desorbed at lower temperatures.[58] At 150 °C, the physisorbed pyridine will desorb from the surface, leaving only the pyridine chemisorbed on the catalyst surface. For silica-magnesia(-copper oxide) systems, this is an assumption based on what is observed for pyridine-FTIR studies of zeolites.[63,64]

The assignment of spectroscopic peaks in the OH-region and of adsorbed pyridine/pyridinium species on, respectively, Lewis and Brønsted acid sites is based on previous pyridine-FTIR studies on silica-magnesia systems ([34,57,60]), clays containing mostly silica and magnesia ([58]), silica-alumina systems ([59]), silica systems ([65]) and zeolites ([64, 66-69]).

Pyridine species adsorbed on different acidic sites show four different absorptions in the 1400-1700 cm^{-1} region.[57] When pyridine is adsorbed on Brønsted acid sites, it is protonated, thus forming a pyridinium ion, which shows two characteristic spectroscopic bands at approximately 1640 cm^{-1} and 1540 cm^{-1}.[58,59] When pyridine is adsorbed on Lewis acid sites, two bands in the ranges 1600-1628 cm^{-1} and 1445-1462 cm^{-1} are observed.[58] The latter band is assigned to contributions from pyridine adsorbed on both Lewis and Brønsted acid sites. It has been shown that higher wavenumbers for these bands correspond to stronger Lewis acid sites of the sample under study.[57] Zeolites often possess strong Brønsted acidic sites ([69]), whereas metal oxides usually contain prevailing Lewis acidity.[59,65] Figure 4 shows the adsorption modes of pyridine on, respectively, a Brønsted and a Lewis acid site. Physisorbed pyridine species show adsorption in the ranges 1580-1600 cm^{-1} and 1442-1455 cm^{-1}, which are partially similar to the ranges in which peaks appear due to pyridine chemisorbed on Lewis acidic sites. Due to the fact that physisorbed pyridine can be more easily desorbed, bands due to the presence of Lewis acidic sites are observed more clearly when spectra are taken at higher temperatures.[58]
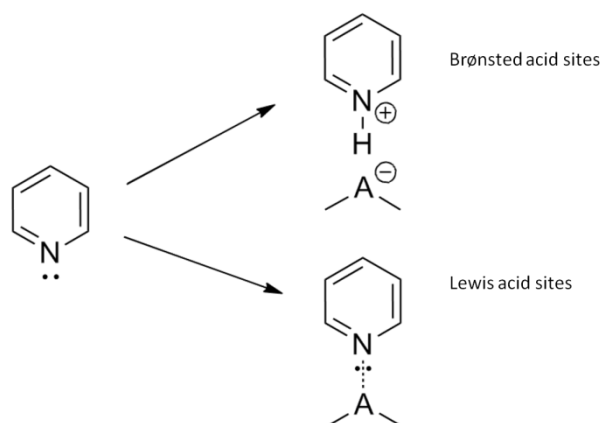
Theory

Figure 4: Adsorption states of pyridine at acid sites

Many publications can be found on the assignment of different hydroxyl groups (OH) in zeolites with FTIR.[67-69] Unfortunately, not much can be found on the nature of hydroxyl groups in silica-magnesia systems and the data which can be found in these studies is sometimes contradictory.[34,60,70] In their pyridine-FTIR study of silica-magnesia systems, prepared via the wet-kneading procedure, Niiyama *et al.* assign a band at 3650 cm^{-1} to acidic OH and bands at 3840 and 3720 cm^{-1} to basic OH. In general terms, it is reported that a band with a higher frequency caused by an OH vibration corresponds to a hydroxyl group with a more basic nature.[34] Kermarec *et al.* observed two different bands due to hydroxyl groups in silica-magnesia systems, prepared from a sol-gel solution, at 3710 and 3670 cm^{-1}. They assigned the band at 3670 cm^{-1} to the presence of OH bonded to tetra-coordinated magnesium and the band at 3710 cm^{-1} to octahedrally coordinated magnesium.[60] Brew *et al.* studied magnesium silicate hydrate gels, prepared via co-precipitation, and observed a band at around 3690 cm^{-1} which they assigned to the Mg-OH stretching vibration in phyllosilicates. The band at 3720 cm^{-1} was assigned by Brew to hydroxyl groups of brucite $Mg(OH)_2$.[70]

2.2.2.2 Deuterated Chloroform-FTIR

In 1979, Paukshtis *et al.* firstly proposed to study basic properties of oxide catalysts, prepared by calcination of the respective hydroxides, via the use of halogen-substituted hydrocarbons, in particular chloroform, as probe molecules for IR spectroscopy.[71] They showed that adsorbed chloroform shows a C-H vibration having lower wavenumbers as compared with non-adsorbed chloroform; moreover it was reported that stronger basic sites cause a shift in the peak due to C-H vibration to lower wavenumbers. Furthermore, Paukshtis *et al.* studied deuterated chloroform, considered better than chloroform, because the C-D vibration does not overlap with the broad band due to O-H stretching observed in the presence of water. They showed that spectra of $CDCl_3$ adsorbed on silica exhibit an absorption band at 2265 cm^{-1}, which is close to the position of the v_{CD} of physisorbed deuterated chloroform at 2264 cm^{-1}. Paukshtis *et al.* also investigated the basic properties of magnesia with deuterated chloroform, thus showing that two bands can be observed with a simultaneous decrease of the frequency of the OH bands of MgO, indicating the adsorption of deuterated chloroform on surface hydroxyl groups. The first band is between 2245 and 2250 cm^{-1} and was assigned to deuterated chloroform interaction on a weak basic site. The second band between 2210 and 2220 cm^{-1} was assigned to strong basic sites.

The experiments performed by Paukshtis to study basic properties of oxide catalysts have been taken as a milestone in the field and have been applied in basicity studies on zeolites ([61,72-75]), metal oxides ([61,74]) and hydrotalcites (MgO-Al$_2$O$_3$ systems) ([76,77]). These more recent studies gave more insight into the nature of the two absorption bands (as reported in Figure 5), thus proposing that deuterated chloroform can be adsorbed on solid catalysts in different ways and this originates different spectroscopic bands.
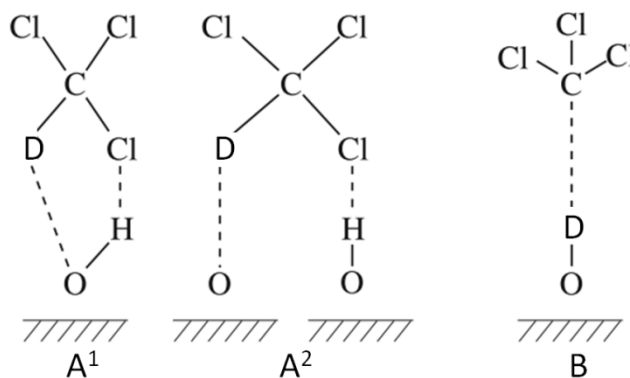
Figure 5: Adsorption states of CDCl$_3$[78]

Based on literature, the band between 2245 and 2250 cm^{-1} is assigned to the adsorption states A^1 and A^2 and indicates interaction of deuterated chloroform with weak basic sites. The deuterium of CDCl$_3$ interacts with one of the lone pairs of the oxygen atom on the catalyst surface. This interaction weakens the C-D bond, thus lowering the vibration wavelength. The band in the region 2210-2220 cm^{-1} is assigned to adsorption state B in Figure 5, originated by the presence of stronger basic sites on the catalyst surface. This kind of basic site interacts with the deuterium of CDCl$_3$ causing a more pronounced weakening of the C-D bond, thus leading to a shift to lower frequencies.[77,78]

2.2.3 Ammonia Temperature Programmed Desorption (NH$_3$-TPD)
In TPD, the strength of active sites on a catalyst surface is measured with the use of probe molecules. Probe molecules form a bond with the active site on the catalyst surface, based on e.g. an acid-base interaction. The strength of this interaction depends on both the nature of the probe molecule and the catalyst surface. When heating the catalyst, energy is transferred to the adsorbed probe molecules, causing them to desorb. The amount of desorbed probe molecules is measured with a mass spectrometer. The temperature at which desorption takes place is known as the desorption temperature, which is thus related to the strength of the bond. Ammonia is commonly used to probe acidic sites in TPD studies. The higher the desorption temperature, the stronger the acid site under investigation.[79]
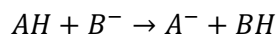
2.2.4 Hammett Indicators
With the use of Hammett indicators, the bulk acid-base properties of a catalyst can be determined by employing a set of indicators with different pK$_a$ values. Each indicator molecule has a certain color in the acidic form and a different color when it is deprotonated. The prepared catalyst is typically suspended in an aprotic solvent and kept in an inert atmosphere to ensure that the employed solvent or air molecules, such as water and carbon dioxide, do not interfere with the acid-base measurements. Commonly used solvents include pentane, hexane or benzene.[80] When one indicator is added to the suspension containing the catalyst, it reacts with the acidic-basic sites of the catalyst; if there is a prevailing presence of basic sites stronger than the indicator pK$_a$, the characteristic color of the basic form of the indicator is observed. All indicators are put in contact with suspensions of the catalyst in a defined order. Following this procedure it is possible to determine a range of pK$_a$ for the basic (or acidic) sites of the sample under investigation. In particular, the basic (or acidic) sites of the catalyst have a pK$_a$ between the pK$_a$ of the last indicator which underwent color change and the first which did not show color change upon interaction with the catalyst.[78,81,82]

The silica-magnesia catalysts studied in this thesis all show prevailing basicity in a benzene suspension. Therefore, the focus in this chapter will be on the study of solid bases with Hammett indicators. The H$_-$ acidity function is one of the most important concepts in the determination of the basicity of solutions and is the counterpart of the H$_o$, which is used in acidic solutions. The H$_-$ acidity

function is defined as a measure of the ability of a basic site to abstract a proton from an acidic neutral solute AH.[83] Tanabe *et al.* proposed to use the H_ function as a measure for the strength of solid bases such as metal oxides and zeolites.[84] Scheme 4 shows the reaction between a molecule AH and a basic site B- on the surface of a solid base. The H_ value is then defined as: $H_- = pK_a - \log ([AH]_s/[A^-]_s)$ wherein $[AH]_s$ and $[A^-]_s$ represent the concentrations of AH and A^- on the surface of the catalyst respectively. The surface exhibits the color of AH once $[AH]_s/[A^-]_s \gg 1$, whereas it exhibits the color of A^- when $[AH]_s/[A^-]_s \ll 1$. When $[AH]_s/[A^-]_s = 1$, the H_ value of the basic sites is equal to the pK_a of the indicator molecule.[78,84]

$$AH + B^- \rightarrow A^- + BH$$

Scheme 4: reaction of indicator molecule AH with basic surface site B

The use of Hammett indicators is an easy and quick method to determine the bulk basicity of a catalyst.[85,86] However, this method has some drawbacks. Firstly, the H_ function is based on the nature of Brønsted basicity and acidity. Oxide surfaces can contain both Brønsted and Lewis basic sites. It has, however, not been proven with certainty that the H_ function for Brønsted bases is also in accordance with the capability of Lewis basic sites. Moreover, the results achieved with this method do not allow distinguishing between the presence of Brønsted and Lewis basicity. The second drawback is experimental. Acidity/basicity is determined by a change of color of the indicators on the surface, thus it is difficult to perform these experiments on colored samples. Moreover, color determination is subject to individual judgment.[78] Also, it is not possible to study the acidic sites of solid bases with this method, because the solid together with the aprotic solvent already have a pH value above 7. This means that in solution the basic properties of the catalyst are prevailing over the acidic properties and therefore, in the case of the silica-magnesia catalysts, for example, acidic sites cannot be measured with the use of Hammett indicators.[78,84,87]

Chapter 3. Experimental

3.1 Catalyst Preparation

The silica-magnesia catalysts were prepared according to two different protocols: wet-kneading and co-precipitation. In the wet-kneading procedure, silica and magnesium hydroxide were prepared separately from their respective precursors, tetraethyl orthosilicate (TEOS) and magnesium nitrate ($Mg(NO_3)_2$). Subsequently, the two oxides were wet-kneaded in water. In the co-precipitation procedure, the two precursors in ethanolic solution were precipitated together via addition of an ammonia/ethanol solution. The silica-magnesia catalysts prepared in the previously described ways were doped with 1% copper oxide via incipient wetness impregnation.

3.1.1 Silica Preparation

Silica spheres, with sizes of around 425 and 30-100 nm respectively, were prepared following a Stöber-like procedure [38] and employed in the wet-kneading procedure. Silica spheres with sizes larger than 1.5 μm were prepared by allowing the growth of Stöber-like silica spheres of around 900 nm in suspension (seed solution). The growth was performed at the laboratories of the Soft Condensed Matter group of the Debye Institute at Utrecht University.

3.1.1.1 Stöber Silica Preparation

Silica spheres, possessing a quite monodisperse size of 425 nm were prepared from 5.24 g TEOS, mixed with 480 mL of a EtOH/NH_3 (5:1 v/v) solution and aged for 24h. Next, the sample was centrifuged at 5000 rpm (revolutions per minute) for 10 minutes to recover the solid and washed once with ethanol. The sample was then dried overnight at 120 °C; the so-prepared silica was used to prepare the catalyst named WK. For the preparation of the silica spheres used in the catalyst named WK-MOD, the ammonia/ethanol solution was prepared by mixing 11.25 g of 25 wt% NH_3 with 230 mL of ethanol in a high density polyethylene (HDPE) bottle. The mixture was heated up until 35 °C while stirring at 250 rpm. Once the desired temperature was reached, 17.3 g of TEOS were added at once and the mixture was aged under stirring for 24h. Afterwards, the solution was neutralized with 8.7 mL of nitric acid and subsequently dried in a rotary evaporator at 55 °C at 120 rpm for 30 min.

3.1.1.2 Synthesis of Large Silica Spheres

Seed Batch Preparation
A seed batch, containing Stöber silica, was prepared. The batch contained 423 mL of ethanol, 45 mL of ammonia (25 wt%) and 32 mL of TEOS. In order to increase the time during which two distinct phases were present, the TEOS was added in two parts; the first part consisted of 20 mL and the second part of 12 mL.

Ethanol was put in a beaker and stirred thoroughly. While stirring, ammonia was added under the fluid surface of ethanol with a long funnel to ensure better mixing. Next, the first part (20 mL) of TEOS was added in a similar way as the ammonia, then the beaker was sealed with parafilm. After 4.5 h the second part (12 mL) of TEOS was added under the surface of the solution and the mixture was stirred for another 22.5 h, yielding a suspension of solid silica in an ammonia/ethanol solution. Then, 200 mL of ethanol were added to the mixture and the solution was stirred for additional 5 minutes. Subsequently, the parafilm was removed to allow for ammonia evaporation overnight.

The next day, the batch was centrifuged at 300 rcf (relative centrifugal force) for 30 minutes, followed by decantation of the ethanol/ammonia solution. Subsequently, the sample was washed with ethanol to remove residual ammonia; then, to hinder silica aggregation, the sample was placed in an ultrasonic bath for a few minutes, followed by addition of more ethanol. Subsequently, the sample was centrifuged again under the same conditions followed by decantation. The sample was suspended in a small amount of ethanol and put in an ultrasonic bath again for a few minutes.

The grade of the suspension of silica spheres (0.079 g/mL) was determined by taking 1000 μL with a Finn pipette and evaporating the ammonia and ethanol under a common halogen lamp. The sample was weighed before and after evaporation of the solution.

The batch was analyzed by taking bright field TEM (Transmission Electron Microscopy) micrographs with the use of a Tecnai 12 apparatus operating at 120 keV. The average particle size was 900 nm.

Growth Step

In a round-bottom flask, 2 mL of the suspension were mixed with 17.1 mL of water, 3.36 mL of ammonia (25 wt%) and 51.3 mL of ethanol. Two syringes with a volume of 100 mL were used: the first one contained 20 mL of TEOS and 40 mL of ethanol, while the other syringe contained 13.64 mL of water, 5.38 mL of ammonia (25 wt%) and 41.0 mL of ethanol. The round-bottom flask containing silica was brought under N_2 atmosphere and the mixture was stirred. The content of the two syringes was added to the round-bottom flask with a continuous flow of 0.28 mL/h during 44 h. Next, the rate was altered to 2 mL/h for another 24 h.

After the growth step, the sample was worked up with the same procedures used after the preparation of the seed solution. The so-achieved silica was stored as a suspension in ethanol; the so-prepared silica was used to prepare the catalyst named WK-BIG.

The sample was analyzed by taking bright field TEM micrographs with the use of a Tecnai 12 operating at 120 keV. The average particle size was 1.8 μm

3.1.2 Mg(OH)$_2$ Preparation

Magnesium hydroxide was prepared by dissolving 6.44g of $Mg(NO_3)_2$ in 50 mL of H_2O. Then, 150 mL of 1M ammonia solution were added dropwise while stirring. The solution was then aged for 24 h at 300 rpm. Afterwards, the sample was centrifuged at 5000 rpm for 10 min, washed once with H_2O and dried at 120 °C overnight.

3.1.3 Wet-Kneading

The wet-kneading procedure involves the mixing of the two or more components in a solvent. In this case, magnesium hydroxide and silica prepared as described above were used for wet-kneading. In all cases, silica had a spherical, Stöber-like morphology. Silica spheres having different particle size were used in the preparation of the wet-kneaded catalysts; in particular, for WK-AER commercial Aerosil 300 (as purchased by Degussa) with a particle size of 20-40 nm was used, for WK-MOD 30-100 nm spheres, for WK quite monodisperse spheres of approximately 425 nm and, finally, for WK-BIG silica spheres, larger than 1.5 μm, were employed in the wet-kneading procedure.

For the wet-kneading of the two components (silica and magnesium hydroxide), the same procedure and the same 1:1 molar ratio was employed for all the catalysts. First, magnesium hydroxide and silica were mixed and crushed in a mortar with a pestle to achieve a homogeneous powder. Consequently, wet-kneading took place in 200 mL of H_2O for 4 h at room temperature. After wet-kneading, the sample was centrifuged at 5000 rpm for 10 min and dried overnight at 120 °C. Then, the sample was calcined at 500 °C for 5h with a temperature ramp of approximately 8 °C/min. With the previously described preparations for silica, four different samples were obtained from the wet-kneading procedure: WK (around 425 nm), WK-MOD (30-100 nm), WK-AER (commercial Aerosil silica 20-40 nm) and WK-BIG (around 1.8 μm).

3.1.4 Co-Precipitation

Co-precipitated catalysts were prepared with the same 1:1 molar ratio for silica and magnesia as used in the wet-kneaded ones. The traditional co-precipitated sample (CP) was prepared by dissolving 2.62g TEOS and 3.22g $Mg(NO_3)_2$ in 200 mL ethanol. The solution was then stirred for 20 min. Next, 240 mL of the $EtOH/NH_3$ (5:1) solution was added and the whole mixture was aged for 24 h. The following day the sample was centrifuged for 10 min at 5000 rpm, washed twice with ethanol and dried at 120 °C overnight. The dried sample was subsequently calcined at 500 °C for 5h with a temperature ramp of approximately 8 °C/min. Another co-precipitated catalyst (CP-MOD) was prepared by modifying the order of addition of the two precursors: first, 2.62 g of TEOS was dissolved in 240 mL $EtOH/NH_3$ (5:1) and silica spheres were allowed to form for 20 min. During these 20 minutes, 3.22 g of $Mg(NO_3)_2$ were dissolved in 200 mL ethanol. After 20 minutes, the $Mg(NO_3)_2$ solution was added to the TEOS and the whole mixture was aged under stirring for 24 h. The next day, a procedure identical to the one employed for CP was used; centrifugation, followed by washing with ethanol, drying and calcination.

3.1.5 Incipient Wetness Impregnation of Copper Nitrate

For all the samples prepared with the previously described procedures, 1 wt% of copper oxide was supported on the silica-magnesia catalysts. To do so, first a copper nitrate solution was prepared by dissolving 1.51g of $Cu(NO_3)_2 \cdot H_2O$ in H_2O in a 10 mL volumetric flask. Furthermore, 0.500 g of SiO_2-MgO were dried under vacuum for 1h at approximately 200 °C. The catalyst was then impregnated with 0.1 mL of the $Cu(NO_3)_2$ solution with a syringe, followed by one hour under stirring to allow for $Cu(NO_3)_2$ to distribute homogeneously. The catalyst was then dried under vacuum at room temperature overnight and, finally, calcined at 500 °C for 5h with a temperature ramp of approximately 8 °C/min. By impregnating all the silica-magnesia catalysts prepared as described in 3.1.3 and 3.1.4 with CuO, five additional catalysts were prepared: CuO/WK, CuO/WK-MOD, CuO/WK-AER, CuO/CP and CuO/CP-MOD.

3.2 Characterization Techniques

3.2.1 Coherent Anti-Stokes Raman Scattering (CARS) Micro-Spectroscopy

Coherent Anti-Stokes Raman Scattering (CARS) micro-spectroscopy measurements were performed at the Max Planck Institute in Mainz with a dual-output laser source (Leukos-CARS, Leukos), providing sub-nanosecond pulses at 32 kHz repetition rate and 300 mW average power. For each position in the sample, a CARS spectrum in the range 3100-600 cm^{-1} was acquired on a cooled CCD (Andor). CARS spectra were acquired with pixel dwell times of 1s. The spatial resolution of the instrument was independently measured to be 0.6 x 0.6 x 3.5 μm^3 and the spectral pitch was 4 cm^{-1} per CCD pixel. Raw CARS spectra were analyzed with custom routines in IgorPro 6.22A (Wavemetrics).

The sample for CARS analysis was prepared as follows: a few micrograms of catalyst were placed on a microscope glass slide of about 1 mm thickness. Afterwards, one drop of pyridine was placed on the sample, then the slide was placed in a vacuum oven and heated with a temperature ramp of 5 °C/min until 150 °C were reached; this temperature was kept for 30 minutes. After this thermal treatment, the glass slide on which the catalyst was deposited was covered by a cover slip with a thickness of approximately 0.1 mm and it was sealed to the glass slide by using clear nail polish; once the nail polish was dry, the sample could be analyzed.

3.2.2 Pyridine-FTIR

Pyridine-FTIR measurements were taken with 25 scans per spectrum on a Perkin Elmer System 2000 with a DTGS detector and a resolution of 4 cm^{-1}. Approximately 15 mg of the wanted catalyst were pressed into a pellet and placed into the pyridine cell. The catalyst was first dried in the cell under vacuum with a temperature ramp of 5 °C/min reaching the desired temperature of 550 °C; IR spectra were taken every 25 °C in the temperature range 50-550 °C. Once 550 °C were reached, this temperature was kept constant for 10 minutes, then the sample was cooled down until 50 °C. At this

temperature, pyridine was allowed to flow on the cell containing the catalyst and, afterwards, the catalyst was left in contact with pyridine for 20 minutes to allow for equilibration with the pyridine atmosphere. Next, the catalyst was put under vacuum for 30 minutes to remove the pyridine present in the gas phase. Subsequently, temperature-programmed desorption was started by raising the temperature with 5 °C/min until 550 °C were reached. After increasing the temperature with 25 °C, this was kept constant for 5 minutes. IR spectra were taken every 25 °C to study the pyridine desorption.

3.2.3 Deuterated Chloroform-FTIR

Deuterated chloroform-FTIR measurements were taken with 25 scans per spectrum on a Perkin Elmer System 2000 with a DTGS detector and a resolution of 4 cm^{-1}. The same cell, as used for the pyridine-FTIR, was employed for the chloroform-FTIR. Instead of drying the catalyst in vacuum as done for the pyridine-FTIR study, a constant N_2 flow was employed to favor the removal of species adsorbed on the catalyst surface. Deuterated chloroform was put in a gas bubbler, which was instated into the N_2 lines. Approximately 15 mg of the catalyst subject to analysis were pressed into a pellet and placed into the cell. First, the cell was put under N_2 atmosphere by flushing it for 20 minutes with a N_2 flow of approximately 243 ml/min. Next, the catalyst was dried in the cell under N_2 flow with a temperature ramp of 5 °C/min until 550 °C were reached, IR spectra were taken every 25 °C in the temperature range 50-550 °C. Once 550 °C were reached, this temperature was kept for 60 minutes and then the sample was cooled down until 50 °C. At this temperature, the flow was adjusted to approximately 99 mL/min and, subsequently, N_2 was allowed to flow into the deuterated chloroform-containing gas bubbler for 30 minutes (spectra were taken after, respectively, 5, 10, 20 and 30 minutes). After 30 minutes, the flow was switched back to a pure N_2 flow of 243 ml/min and temperature programmed desorption was started by raising the temperature with 5 °C/min until 550 °C were reached. The cell containing the catalyst was then kept at 550 °C for 10 minutes. Spectra were taken every 25 °C to study deuterated chloroform desorption.

3.2.4 Ammonia-Temperature Programmed Desorption

TPD measurements were performed on a ASAP2920. Typically 0.200g of sample were placed in a quartz reactor. First, the catalyst was dried in the apparatus with a temperature ramp of 5 °C/min to a maximum temperature of 600 °C. Subsequently, it was cooled down to 100 °C. At this temperature NH_3 pulses of 25.31 cm^3/min were applied. The sample was then heated to 600 °C with a ramp of 5 °C/min to study NH_3 desorption.

3.2.5 Hammett Indicators

A 1000 mL three-neck round-bottom flask, filled with dry molecular sieves and benzene was flushed to remove air molecules and was left in argon atmosphere to obtain dry benzene. Seven solutions were prepared by weighing 0.025 g of each indicator, then adding it to a 25 mL volumetric flask subsequently filled with benzene dried as previously described. The indicators used were (in order of growing pk_a): Bromothymolblue, Phenolphthalein, 2,4-Dinitroaniline, 4-Chloro-2-nitroaniline, 4-Nitroaniline, 4-Chloroaniline and Diphenylmethane.[78]

For every test, typically 0.1 g of catalyst was dried in a two-neck round-bottom flask under vacuum at 200 °C overnight. Then, the round-bottom flask was brought in an argon atmosphere and 2 mL of dry benzene were added on the catalyst with a syringe. Next, a few drops of indicator solution were added and a color change, if present, was observed. The flask with sample, benzene and indicator solution was then stored under argon for 24 h to confirm the possible color change.

Chapter 4. Results and Discussion

4.1 Catalyst Synthesis

Table 1 shows an overview of the prepared catalysts in this thesis, with for each catalyst the preparation method and corresponding name to which will be referred in this thesis. The preparation method for each catalyst as described in Table 1 was followed by calcination at 500 °C.

Table 1: Overview of the prepared catalysts employed in this thesis.

Catalyst	Preparation
WK	Wet-kneading of silica spheres of 425 nm and $Mg(OH)_2$ (H_2O)
WK-MOD	Wet-kneading of silica spheres of 30-100 nm and $Mg(OH)_2$ (H_2O)
WK-AER	Wet-kneading of silica spheres of 20-40 nm and $Mg(OH)_2$ (H_2O)
WK-BIG	Wet-kneading of silica spheres of 1.8 μm and $Mg(OH)_2$ (H_2O)
CP	Co-precipitation of TEOS and $Mg(NO_3)_2$ (NH_3/EtOH)
CP-MOD	TEOS (NH_3/EtOH) for 20 min, followed by co-precipitation with $Mg(NO_3)_2$ (NH_3/EtOH)
CuO/WK	Impregnation of WK with 1 wt% CuO
CuO/WK-MOD	Impregnation of WK-MOD with 1 wt% CuO
CuO/WK-AER	Impregnation of WK-AER with 1 wt% CuO
CuO/CP	Impregnation of CP with 1 wt% CuO
CuO/CP-MOD	Impregnation of CP-MOD with 1 wt% CuO

4.2 Bulk Characterization Techniques

Pyridine-FTIR (section 4.2.1.1) and ammonia-TPD (section 4.2.1.2) were employed to study the acidic properties and Hammett indicators (section 4.2.2.1) and deuterated chloroform-FTIR (section 4.2.2.2) were used to study the basic properties of the prepared catalysts as described in section 4.1. Catalyst WK-BIG was prepared specifically to study with spatially-resolved techniques and was thus not studied with bulk characterization techniques.

4.2.1 Acidity Study

4.2.1.1 Pyridine-FTIR

The spectra shown in Figure 6 for the catalyst WK-MOD taken during the drying process (on the left) and during TPD of pyridine (on the right) provide an example of the variation in absorbance with increasing temperature. Generally, while increasing the temperature during the drying process, it is observed that multiple bands for the different OH groups appear upon water desorption. During the TPD step, pyridine is progressively desorbed when increasing the temperature. The strength of acidic sites in the catalysts determine the temperature at which pyridine is desorbed.[65]The results achieved via pyridine-FTIR study are presented in three different sections for convenience. The first section focuses on the study of the OH-region (3500-3800 cm^{-1}) of the catalysts. In this case, the shown spectra refer to the drying procedure taking place before pyridine application to the samples. These results are described in chapter 4.2.1.1.1 In the second part (chapter 4.2.1.1.2) the focus of the analysis is on the region 1400-1700 cm^{-1}, where different bands appear due to pyridine adsorbed on the acidic sites of the various catalysts. Chapter 4.2.1.1.3 studies the influence of CuO on the acidity of the silica-magnesia systems.
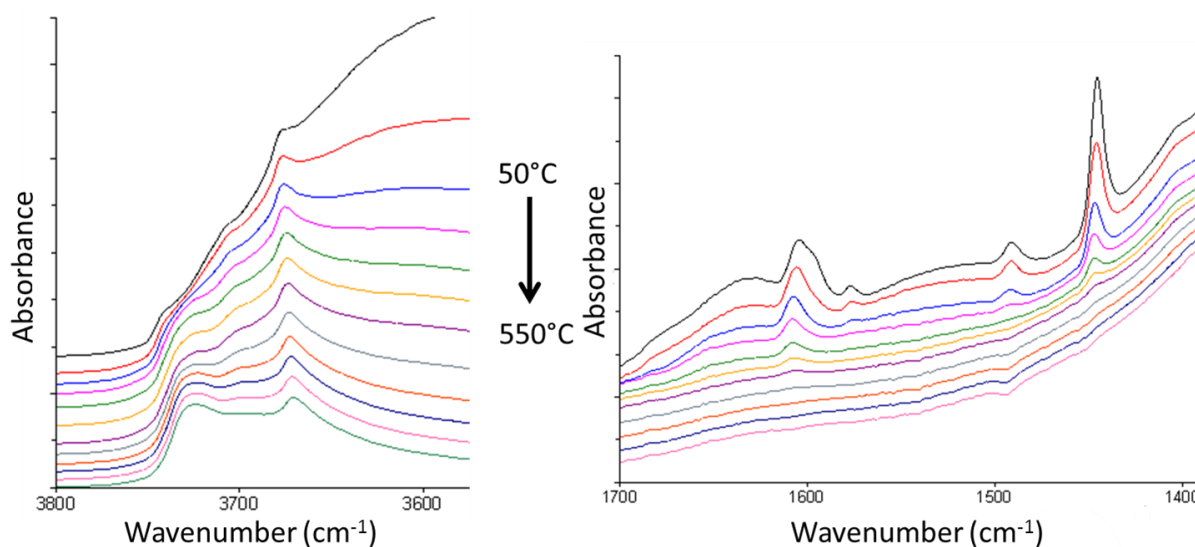

Figure 6: Images showing the evolution of FTIR spectra during the drying process (left) and pyridine TPD (right)for the catalyst WK-MOD with increasing temperature

4.2.1.1.1 OH-region

During the drying process, residual adsorbed water molecules desorb from the catalyst surface, thus leaving exposed hydroxyl groups on the surface of the silica-magnesia catalysts. These groups give rise to bands in the region 3500-3800 cm^{-1}. Figure 7 shows the OH-region for the single oxides silica and magnesia and WK-AER under equal conditions. From the figure, it can be seen that for magnesia only the peak at 3730 cm^{-1} can be observed; furthermore, a peak at 3730 cm^{-1} was reported for hydroxyl groups with a basic character in brucite $Mg(OH)_2$.[70] Silica shows only a broad band, to which, probably, different peaks are contributing, in the OH region with the maximum value at 3700 cm^{-1} already assigned to isolated silanols.[88] Moreover, in literature, peaks shifted to higher

wavenumbers are often explained referring to a more basic character, whereas a lower wavenumber indicates more acidic OH groups.[34]

The peak at 3670 cm^{-1} was not observed for the single oxides and seems to appear only when both silica and magnesia are present. Kermarec *et al.* stated that in silica-magnesia systems, prepared from a sol-gel solution, this peak is related to the presence of tetra-coordinated magnesium. Octahedral coordination of the magnesium atoms would then lead to the presence of a peak at 3710 cm^{-1}.[60] In addition, the IR spectrum of Antigorite (a mineral with chemical formula $Mg_3Si_2O_5(OH)_4$) shows only a sharp peak at 3670 cm^{-1}.[89] The molecular formula suggests that many interactions between magnesium, silicon and oxygen atoms are present in the mineral. This leads to the assignment of the peak at 3670 cm^{-1} to hydroxyl groups bonded to both a magnesium and a silicon atom. Further discussion on the assignment of the peak at 3670 cm^{-1} can be found in section 4.4 of this thesis.
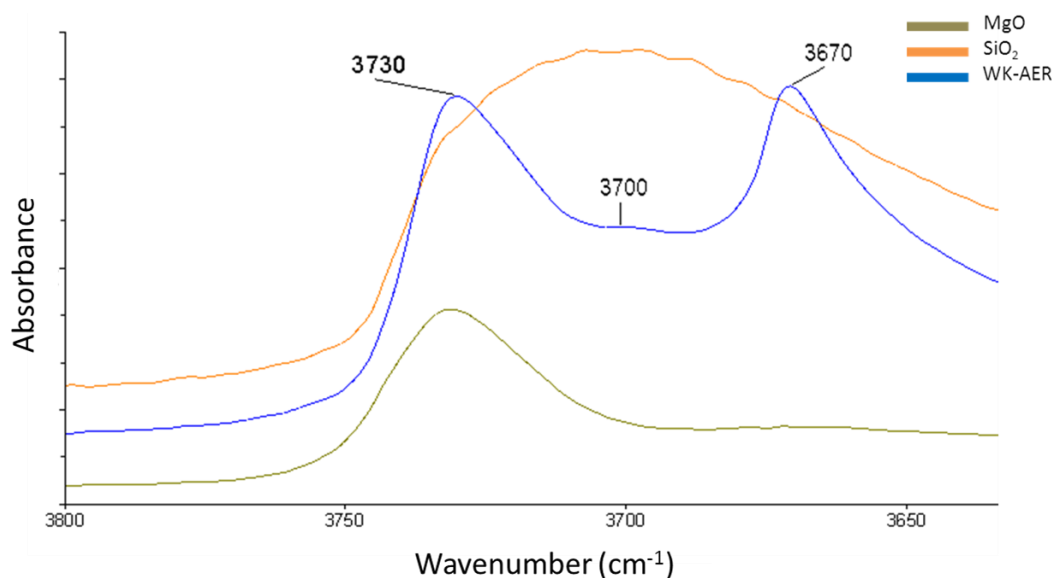

Figure 7: OH region of the FTIR spectra at 550 °C during catalyst drying showing WK-AER, silica and magnesia

Figure 8 shows the OH region for the five silica-magnesia catalytic systems at 550 °C (highest temperature reached during drying). Three distinct peaks can be observed in this spectroscopic range at approximately 3730, 3700 and 3670 cm^{-1}. All three peaks can be seen for WK-MOD and WK-AER, while the CP catalyst shows only one intense absorption around 3730 cm^{-1}. The WK catalyst shows a quite broad band over the entire range considered. This band seems to be due to the overlap of the three considered peaks, with a slightly more pronounced absorption around 3670 cm^{-1}. A different situation was observed for the CP-MOD catalyst, which shows only a broad band, characterized by quite low absorbance. Possibly this is due to a lower abundance of available OH groups. The assignment of the peak at 3670 cm^{-1} to hydroxyl groups bonded to both a magnesium and a silicon atom explains the difference in intensity observed for this peak when comparing the three wet-kneaded samples WK, WK-MOD and WK-AER. These three samples differ in silica sphere size: WK-AER contains the smallest silica spheres (20-40 nm) and, therefore, more hydroxyl groups at the silica-magnesia surface can be present as compared with WK-MOD and especially WK, which contains significantly larger silica spheres (approximately 425 nm). The information from the IR spectrum of the mineral does raise questions about the result for the CP catalyst. The CP catalyst only shows an intense peak around 3730 cm^{-1}, (assigned to basic OH present in brucite $Mg(OH)_2$), but no peaks around 3700 or 3670 cm^{-1}. This is unexpected, since this catalyst, prepared by co-precipitating the silica- and magnesia precursor, is expected to possess the highest amount of silicon-magnesium interactions and, thus, high intensity at 3670 cm^{-1}. Possibly the morphology of the CP

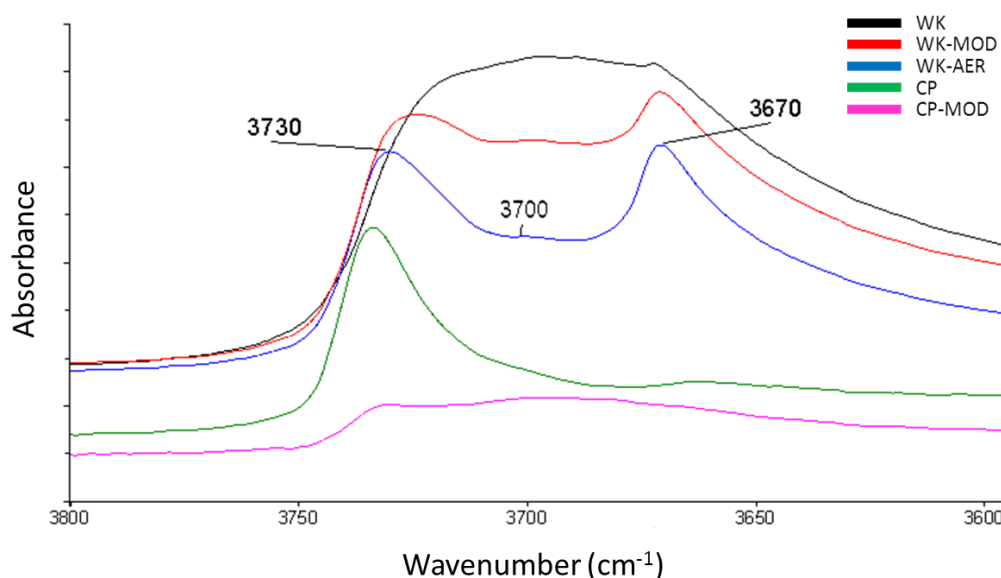catalyst only allows the presence of magnesium-bonded hydroxyl groups, explaining the peak around 3730 cm^{-1}.

Figure 8: OH region of the FTIR spectra at 550 °C during drying showing the five different silica-magnesia catalytic systems.

4.2.1.1.2 Pyridine-Region

Once the catalysts were dried, the samples were exposed to pyridine at 50 °C. In Figure 9, spectra at 150 °C are reported for the five different samples. It is assumed that at this temperature all physisorbed pyridine has been removed, leaving only the chemisorbed pyridine on the catalyst surface. Four bands, corresponding to different ring deformation vibrations of pyridine coordinated on Lewis acid sites were observed.[58] The band at 1490 cm^{-1} corresponds to the summation of both Lewis and Brønsted acidity contributions.[58] No peaks corresponding to pyridinium ions generated on Brønsted acid sites were observed for any of the five catalysts (1540 cm^{-1} and 1640 cm^{-1}), indicating that the hydroxyl groups are not acidic enough to protonate the pyridine molecules.[58] López *et al.* studied the acidic and basic properties of silica-magnesia systems, prepared via the sol-gel procedure, with varying ratios of silica and magnesia and reported similar results, observing only Lewis acidity present in silica-magnesia systems and no Brønsted acidity.[90] When comparing the different silica-magnesia catalysts, it can be seen that CP shows the peaks with the highest intensity, indicating that this catalyst contains the highest amount of acidic sites. On the other hand, WK was observed to have the lowest intensity for the bands due to pyridine adsorbed on Lewis acid sites. Comparing the intensity of the peak at approximately 1445 cm^{-1} (highest intensity in all cases) from Figure 9 for the five silica-magnesia catalysts, the following order for the amount of acidic sites can be derived: CP > WK-AER > WK-MOD ≈ CP-MOD > WK. It is difficult to distinguish between the WK-MOD catalyst and the CP-MOD catalyst, because the band at 1445 cm^{-1} is more intense for the CP-MOD, whereas the bands at 1490 and 1604 cm^{-1} have a higher intensity in the WK-MOD spectra.

In section 1.3 it was proposed that a high yield of ethylene in the catalytic performance could be an indication for a high concentration of acidic sites in the catalyst. The catalytic performances of the silica-magnesia systems are shown in Figure 2 in section 1.3.3. CP yields the highest amount of ethylene, which is in line with the pyridine-FTIR results, as CP contains the highest concentration of acidic sites according to these results. Also, WK shows the lowest production of ethylene, which is in accordance with pyridine-FTIR results showing the lowest concentration of acidic sites. For all five catalysts, the pyridine-FTIR results are in line with the ethylene production, except for the results for the CP-MOD catalyst, since its low amount of acidic sites does not correspond with its large ethylene production.
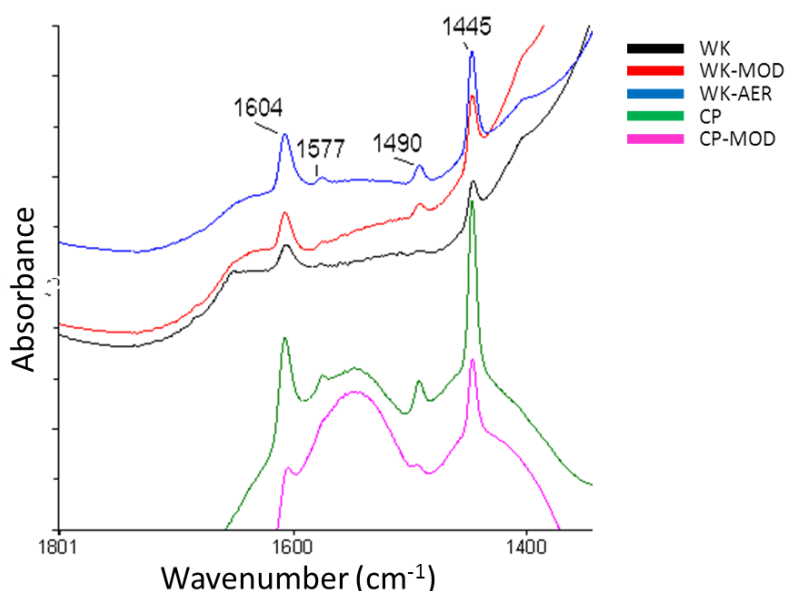
Figure 9: Pyridine region of the FTIR-spectra at 150 °C during temperature programmed desorption for the silica-magnesia catalysts

The strength of acidic sites can be derived from the temperature at which pyridine is completely desorbed from the catalyst surface.[65] Pyridine is desorbed at higher temperatures when chemisorbed on stronger acidic sites. The spectra (not shown here for brevity) show a significant difference in the temperature at which the pyridine peaks cannot be observed. In Table 2, this temperature is reported for the five silica-magnesia catalysts. In particular, it can be seen that CP contains the strongest acidic sites (pyridine peaks disappearance at 475 °C). The order for the strength of acidic sites is quite similar to what was observed for the amount of acidic sites. The only exception is to be found in the CP-MOD catalyst, having the lowest temperature (300 °C) of pyridine desorption. A possible explanation for this relates to the synthesis method for CP-MOD as described in section 3.1.4, in which silica spheres are co-precipitated with a magnesium nitrate solution. This resulted in a low amount of hydroxyl groups, as shown in Figure 8, and in weak acidic sites. These two observations suggest a low interaction between the silica- and the magnesia phase, thus a low amount of chemical bonds between the two phases.

Table 2: Temperatures of complete disappearance of the peaks due to adsorption of pyridine on acidic sites of the silica-magnesia catalysts

Sample	Temperature of complete disappearance of pyridine (°C)
WK	350
WK-MOD	400
WK-AER	450
CP	475
CP-MOD	300

In order to compare the FTIR-spectra for the catalysts with those of the single oxides silica and magnesia, pyridine-FTIR experiments have also been performed on silica and magnesia. Silica spheres, which were employed in the synthesis of WK-MOD (30-100 nm), were used in these measurements. The results are given in Figures 10 and 11, in which the pyridine-region for silica and magnesia are shown during TPD at 100, 300 and 525 °C. It is observed that pure silica contains a quite low amount of acidic sites, given that the peaks at approximately 1598 and 1445 cm^{-1} have low

intensities and, furthermore, they cannot be observed at temperatures higher than 100 °C , thus they are characterized by a quite weak strength as compared with acidic sites observed for silica-magnesia catalysts. These results are in line with the observations done by Parry *et al.* during a pyridine-FTIR study on fumed Cab-O-Sil silica with a typical surface area of 200 m^2/g.[65] They observed similar peaks at 1447 and 1599 cm^{-1}, which were attributed to ring deformation vibrations of pyridine weakly bound to Lewis acidic sites. They also observed that pyridine was desorbed at 150 °C, which is in line with the results shown in Figure 10.
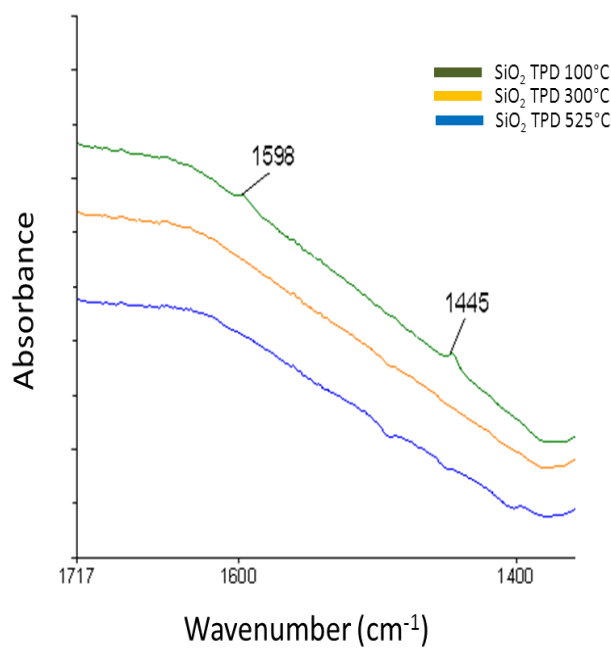

Figure 10: FTIR spectra at 100, 300 and 525 °C during TPD, showing the pyridine-region for silica

In contrast, relatively intense peaks can be observed for the magnesia in the pyridine region. The band around 1653 cm^{-1} corresponds to adsorbed water molecules and disappear when increasing the temperature. The peaks at 1601, 1508 and 1445 cm^{-1} correspond to pyridine adsorbed on Lewis acidic sites. Compared to the peaks observed for silica, these show higher intensity and disappear at higher temperatures (the peak at 1508 cm^{-1} is still present at 525 °C). The band at 1508 cm^{-1} is not present in the spectra for the silica-magnesia catalysts and is attributed to ring deformation vibrations of pyridine chemisorbed on strong Lewis acid sites.[58] These results show that magnesia, despite the fact of being an oxide with mainly basic character, has more acidic sites than silica. Furthermore, it can be seen that all silica-magnesia catalysts show higher intensity for the pyridine adsorbed peaks, thus implying that new (and stronger) acidic sites are generated when both components are present at the same time. To the best of our knowledge, results for a pyridine-FTIR study on magnesia have not been reported. However, the positive influence on the acidity due to addition of magnesia to silica has been shown often in the study of silica-magnesia systems prepared via the sol-gel procedure.[60,90] Therefore, although magnesia is usually considered a basic oxide, it is considered to increase the acidic properties in catalytic systems.
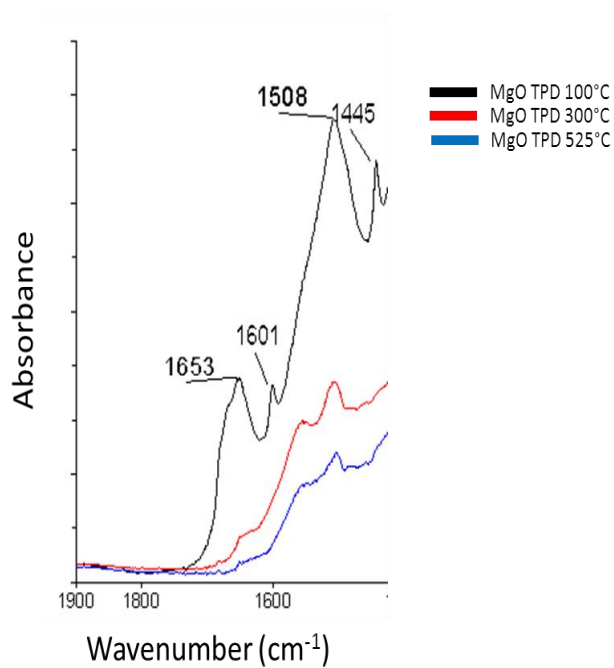
Figure 11: FTIR spectra at 100, 300 and 525 °C during TPD, showing the pyridine-region for magnesia

4.2.1.1.3 Influence of CuO

All the previously described silica-magnesia catalysts were doped with CuO. In order to determine the influence of CuO-promotion on acidic and basic properties of the catalysts, pyridine-FTIR experiments were performed for the CuO-containing catalysts. For each silica-magnesia catalyst, the spectra before and after CuO-doping for the OH- (Figure 12) and pyridine-region (Figure 13) are reported.

In the OH-region, it can be seen that the intensity of the peaks due to the hydroxyl groups decreases in all cases upon doping with CuO, which is explained considering that these surface hydroxyl groups act as anchoring points for the CuO. Figure 12 shows that the ratio in intensity for the three different hydroxyl peaks decreases in a similar way for all the samples upon CuO-doping, except for the WK-MOD and CP-MOD catalysts. In these catalysts, it seems that CuO has a preference for binding on the hydroxyl groups with absorption at 3730 cm^{-1}, which were previously attributed to OH groups present on the magnesia moiety. This is not completely in line with previous work done on these catalysts in this group, in which TEM (transmission electron microscopy) and EDX (energy dispersive X-ray) spectroscopy showed that CuO particles were both present on the silica and magnesia surface and showed no preference for one.[91] The reason for the observed different behavior for WK-MOD and CP-MOD is still under investigation.
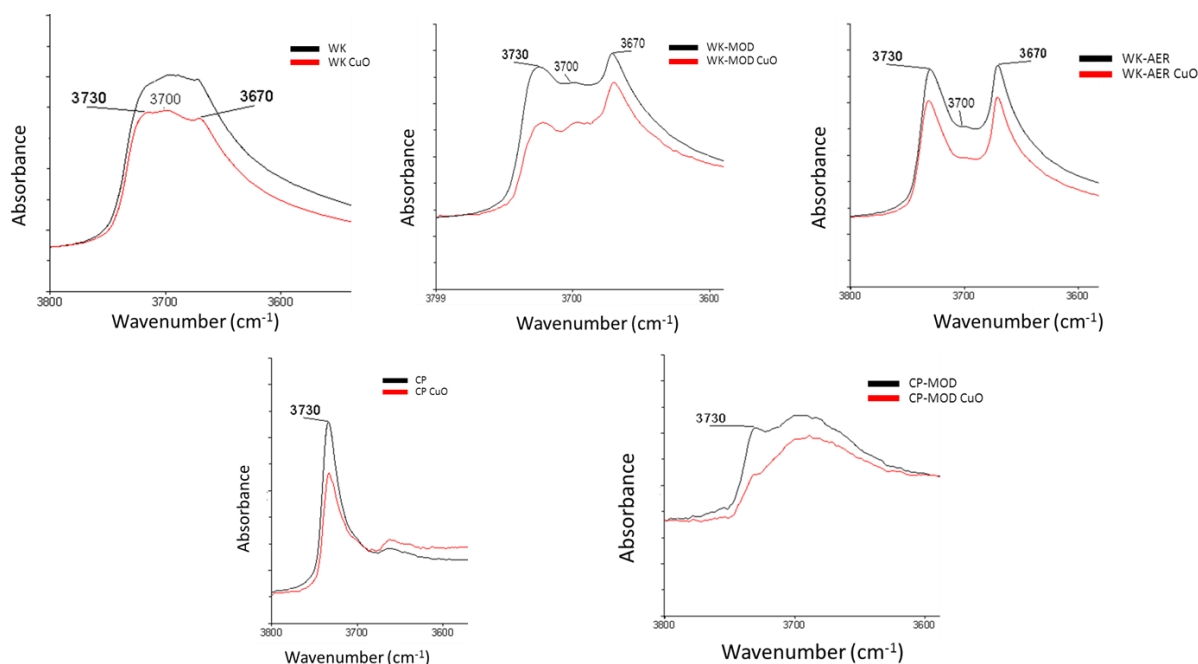

Figure 12: FTIR-spectra at 550 °C during drying showing the OH-region for the silica-magnesia catalysts in comparison with the corresponding CuO-doped catalysts

The spectra in the pyridine-region for the five catalysts show that the influence of CuO on the acidic properties varies significantly among the different catalysts, as can be seen in Figure 13. In particular, it can be observed that CuO-promotion has no significant influence on the acidic properties of the WK-MOD and WK-AER catalysts: the four bands assigned to pyridine adsorbed on Lewis acidic sites in the CuO-promoted catalysts show similar position and only slightly lower intensity compared with the unpromoted silica-magnesia systems. Furthermore, in Table 3, it can be seen that the temperatures at which pyridine is completely desorbed from the surface for the CuO-doped catalysts is higher in the case of WK-MOD and WK-AER. This indicates that despite the fact that the amount of acidic sites is unchanged upon CuO-promotion, some stronger sites are generated. This observation possibly can be explained by Zaccheria *et al*, who recently published a paper in which the influence of dispersed CuO particles on a silica surface on the acidic properties is studied. Pyridine-FTIR studies showed that two peaks were present in the pyridine-region for the CuO-promoted silica surface at

1453 and 1611 cm^{-1}, attributed to pyridine adsorbed on Lewis acidic sites. Moreover, they observe a significant increase in acidity due to the CuO and this increase in acidic behavior is ascribed to coordinative unsaturation of the very small CuO particles.[92] A different scenario was observed for WK: CuO-promotion in this case significantly reduces the amount of acidic sites, thus no peaks due to adsorbed pyridine could be observed for this catalyst. When considering the two co-precipitated catalysts in Figure 13, it can be seen that adsorbed-pyridine peaks show significantly lower intensity in the case of the CuO-doped samples as compared with the silica-magnesia ones. Also, as can be seen in Table 3, the strength of the acidic sites present in the CuO-containing catalysts is significantly lower, especially for the CP catalyst.
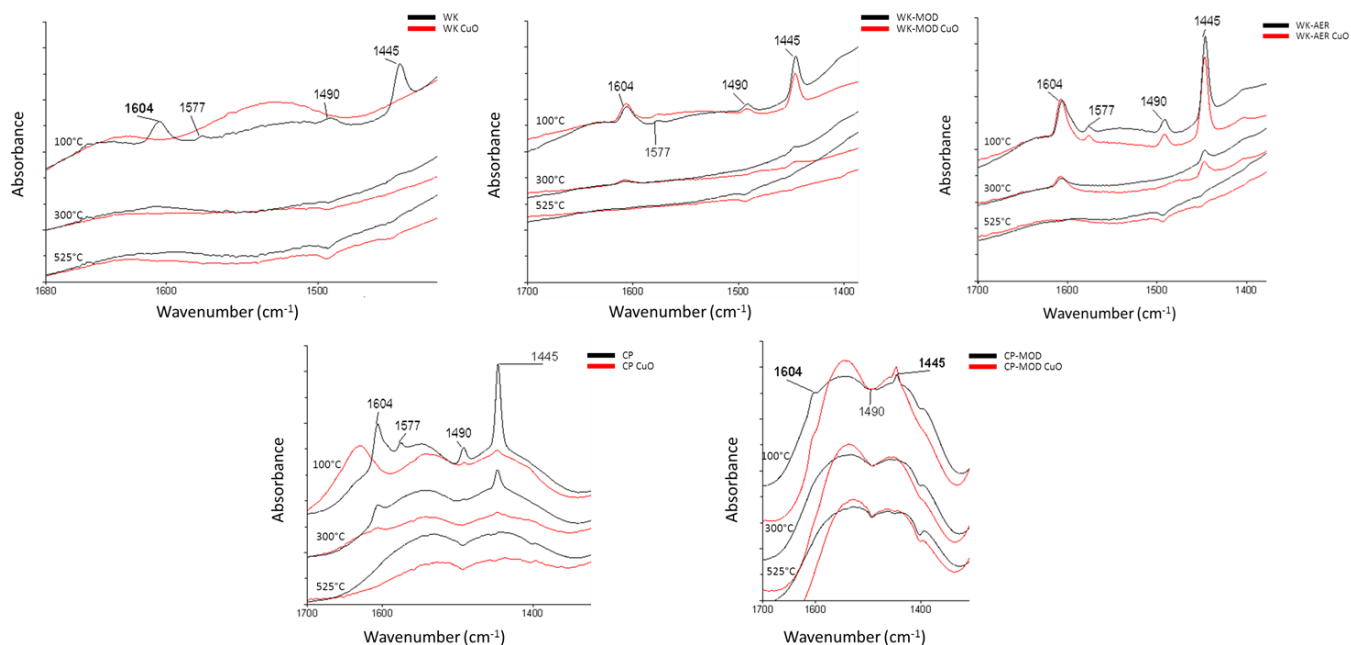

Figure 13: FTIR spectra at 100, 300 and 525 °C during TPD in the pyridine-region showing a comparison between the silica-magnesia catalysts and the CuO-doped corresponding catalyst

When comparing the results of the pyridine-FTIR with the catalytic performances in Figure 2, the decrease in amount of acidic sites for the co-precipitated samples can be correlated with their decrease in ethylene production. Thus, the ethylene yield is an indication for the concentration of acidic sites in the catalyst. However, the pyridine-FTIR results show that the CuO-promoted catalysts WK-MOD and WK-AER contain a higher concentration of acidic sites than the co-precipitated ones, yet their ethylene production is lower as compared with the co-precipitated catalysts. This might indicate that the concentration of basic sites also influence the catalytic performance and that the concentration of acidic sites in a catalyst is not a direct measurement for the ethylene production.

Table 3: Temperatures of complete disappearance of pyridine for the silica-magnesia catalysts[1]

Sample	Temperature of complete disappearance of pyridine (°C)
CuO/WK	-
CuO/WK-MOD	450
CuO/WK-AER	475
CuO/CP	375
CuO/CP-MOD	275

1: The temperature for the CuO/WK catalyst is missing, because the FTIR-spectra do not show peaks corresponding to pyridine adsorbed on acidic sites

4.2.1.2 Ammonia-Temperature Programmed Desorption (NH₃-TPD)

During TPD, the amount of ammonia (NH_3) desorbed (as function of the temperature used) upon heating can be used as a measure of the amount and strength of acidic sites of a solid catalyst.[93] Figures 14, 15 and 16 show the results for ammonia-TPD measurements of the ten catalysts. NH_3 desorbed at a relatively low temperature is an indication of weak acidic sites in the catalyst.[85] Moreover, the integral of the peak observed in TPD can be used to calculate the amount of acidic sites.[93] The assumption in TPD is that one NH_3 molecule adsorbs on a single acidic site. In addition, the width of a specific peak is proportional to the distribution of strengths of the acidic sites.[94] The ammonia TPD curve of zeolites usually presents two distinct peaks, indicating the existence of at least two groups of active sites with different ranges in acidic strength.[95] The temperature of desorption is different for each zeolite, but a desorption around 400 °C is common in zeolites ZSM-5 and Y.[96] NH_3-TPD shows sites with different acidic strength, but it cannot distinguish between Brønsted and Lewis acidity.[95,97] In all cases, a quite broad distribution of acidic sites is observed; this, connected with the scarcely known nature of acidic sites found in silica-magnesia(-copper oxide) materials, makes it impossible to attribute specific intensities of e.g. weak and strong acid sites. For these reasons, it was decided to integrate the whole peaks in order to calculate the total concentration of acidic sites in mmol/gram for the different catalysts.

4.2.1.2.1 Silica-Magnesia Systems

Ammonia-TPD results for the five silica-magnesia catalysts are shown in Figure 14 and the calculated amount of acidic sites are reported in Table 4. The peak integrations are given in cm^3/g, which is the volume of desorbed ammonia per gram of catalyst at the given temperature. With the ideal gas law, given in Scheme 5, the amount of desorbed in ammonia can be calculated in mmol. Assuming that one NH_3 molecule adsorbs at one acidic site, the concentration of acidic sites is equal to this amount.

$$n = \frac{1000 \times p \times V}{R \times T}$$

Scheme 5: Ideal gas law formula to calculate the amounts of mmol from the given volume (m³), in which p equals a standard pressure of 101325 Pa (1 atm), R equals a constant of 8.3145 J/mol·K and T equals the standard temperature 273 K. The factor of 1000 is added to convert mol into mmol (n).

From Figure 14, it can be clearly seen that CP, showing the highest intensity, is the most acidic catalyst and WK, showing a low intensity, is the least acidic one, which is in line with the pyridine-FTIR results. With the calculated amounts of acidic sites, the order for the five silica-magnesia catalysts can be derived: CP > CP-MOD ≈ WK-AER > WK-MOD > WK. These results are in accordance with the observed ethylene production (see section 1.3.3) and with the results from the pyridine-FTIR, except for the position of CP-MOD, which appears to be more acidic than WK-MOD and shows a similar amount of acidic sites compared with WK-AER. A possible explanation might be that the acidic sites in CP-MOD are only accessible to small molecules such as NH_3, but not to pyridine.
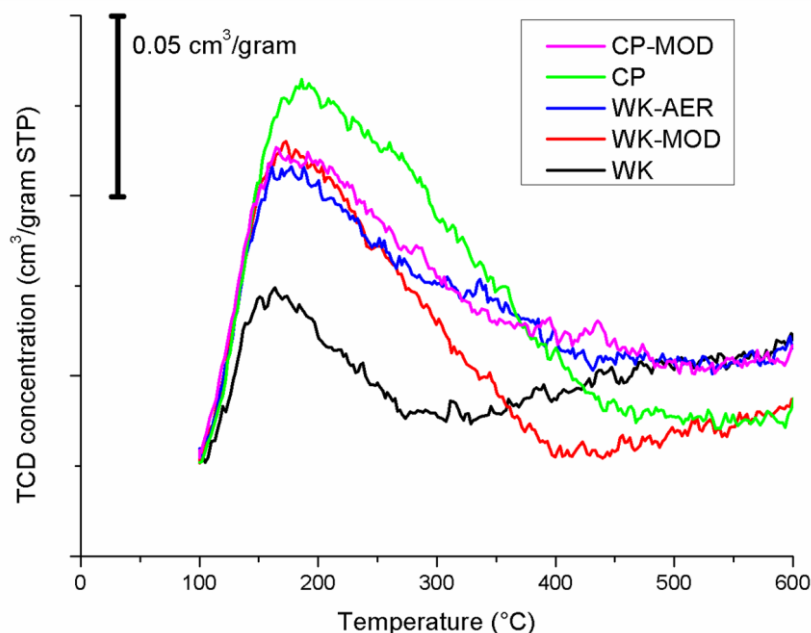
Figure 14: TPD results for the silica-magnesia catalysts

Table 4: Calculated concentration of acidic sites for all catalysts based on TPD results

SiO$_2$-MgO catalyst	Concentration acidic sites (mmol/gram)	CuO/SiO$_2$-MgO catalyst	Concentration acidic sites (mmol/gram)
WK	0.145	CuO/WK	0.129
WK-MOD	0.219	CuO/WK-MOD	0.180
WK-AER	0.234	CuO/WK-AER	0.270
CP	0.268	CuO/CP	0.134
CP-MOD	0.242	CuO/CP-MOD	0.155

4.2.1.2.2 Influence of CuO

The CuO-doped silica-magnesia catalysts were also tested with NH$_3$-TPD. Figure 15 shows the results for the CuO-promoted catalysts and the corresponding calculated concentrations of acidic sites in mmol/gram are reported in Table 4. The CuO/WK catalyst was observed to have the lowest concentration of acidic sites, as in the case of the unpromoted catalysts; on the other hand, CuO/CP is not the sample with the highest amount of acidic sites. According to ammonia-TPD measurements, CuO/WK-AER is observed to be significantly more acidic than the other CuO-containing catalysts. The amount of acidic sites for the CuO-doped catalysts follows the order: WK-AER > WK-MOD > CP-MOD > CP ≈ WK. These results are not completely consistent with the results from the pyridine-FTIR, as they show a significant larger decrease in acidic sites for WK. However, the decrease in amount of acidic sites for the co-precipitated samples upon CuO-promotion is confirmed by the results from the pyridine-FTIR. Moreover, both methods show that the CuO-promoted WK-AER is the most acidic catalysts as compared with the other doped systems, showing both the highest concentration of acidic sites and the strongest sites present in the catalyst.
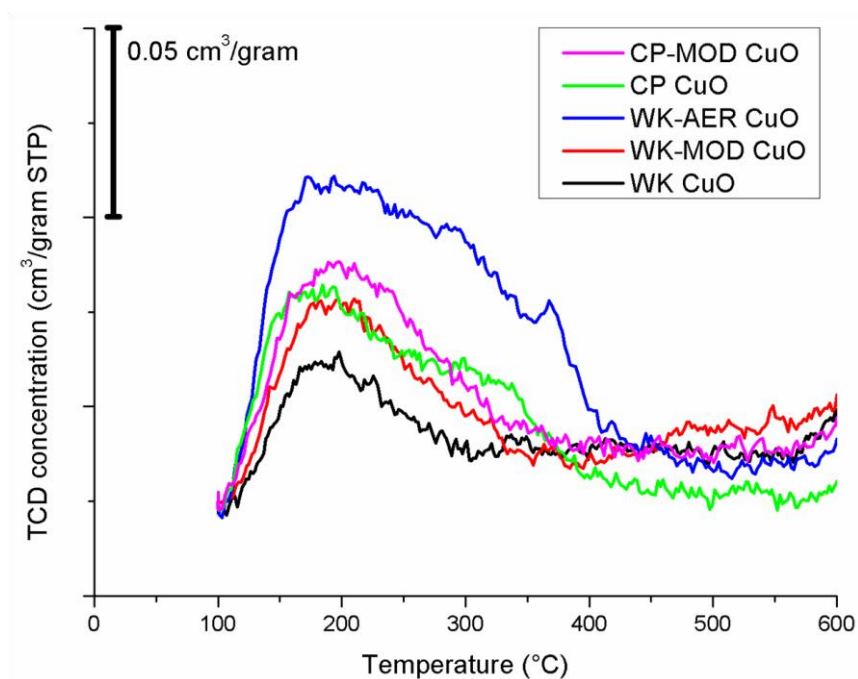
Figure 15: TPD results for the CuO-doped silica-magnesia catalysts

In order to have a clear overview of the influence of copper oxide on the acidity of the different catalysts, Figure 16 shows the comparison between promoted and unpromoted catalysts individually. Notably, the effect of CuO-promotion is significantly different for the three wet-kneaded catalysts. Upon doping with CuO, the concentration of acidic sites of the WK catalyst decreases slightly (0.15 vs 0.13 mmol/g). However, the top of the peak for CuO/WK is shifted to a higher temperature, indicating that the acidic sites become stronger upon CuO-doping. These results significantly differ with what was observed with pyridine-FTIR. It is possible that some of the acidic sites are not accessible to pyridine, but only to smaller molecules such as ammonia. WK-MOD loses a certain amount of acidic sites upon CuO-promotion (0.22 vs 0.18 mmol/g). WK-AER however, shows an increased amount of acidic sites with the addition of CuO. Table 4 shows that the concentration of acidic sites in WK-AER increases (0.23 vs 0.27 mmol/g). The co-precipitated samples show decreased acidity with the addition of CuO, especially in the case of the CP catalyst, which loses half of its acidic sites (0.27 vs 0.13 mmol/g) as can be seen in both Figure 16 and Table 4. Also the CP-MOD loses quite some acidic sites (0.24 vs 0.16 mmol/g). Thus, WK-AER is the only catalyst for which the concentration of acidic sites increases upon CuO-promotion. For the other catalysts, the amount of acidic sites decreases upon CuO-doping; in the case of WK, this decrease is much less pronounced than for the remaining three samples.
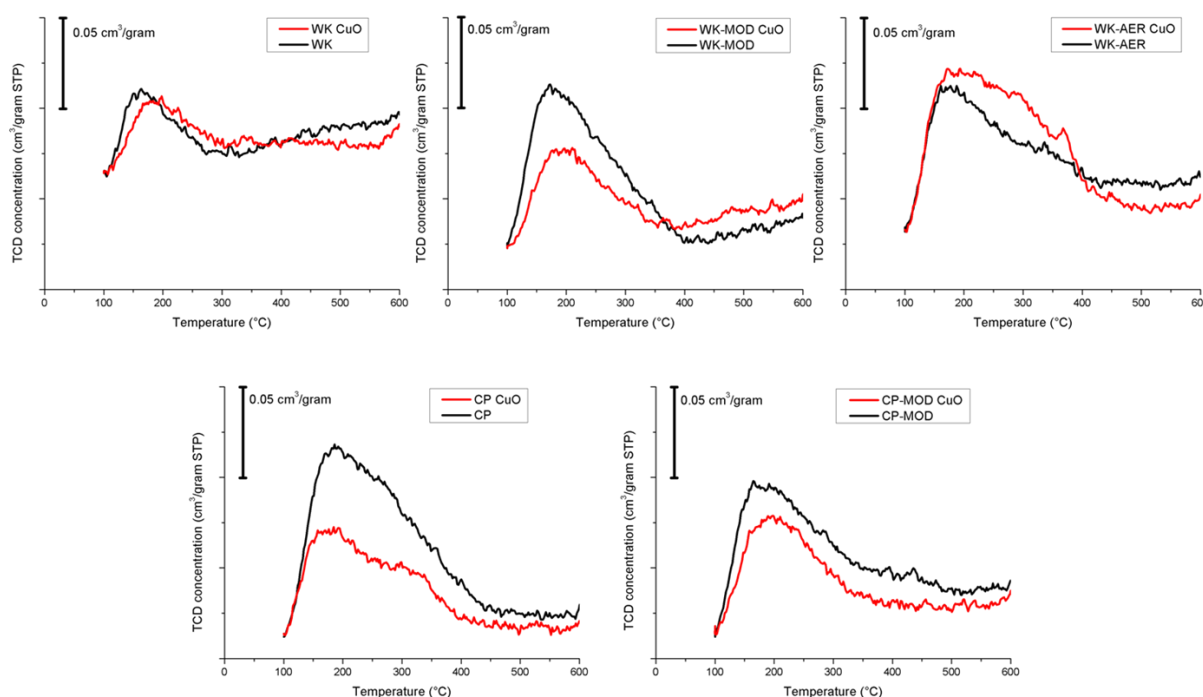
Figure 16: TPD results for every catalyst with and without CuO-promotion

4.2.2 Basicity Study

This section shows the results from the Hammett indicator study and the deuterated chloroform-FTIR. Results regarding the basic hydroxyl groups on the surface were already dealt with in Section 4.2.1.1.1.

4.2.2.1 Hammett Indicators

Table 5 reports the results for the Hammett indicator study. The indicator solutions initially show the color of the acidic form, so a color change indicates the prevailing formation of the basic species of the indicator due to deprotonation on the catalyst surface. The experiments were performed by adding the indicator solution to a suspension of the catalyst in benzene and the color (due to either the acidic or basic indicator form) was observed upon adsorption of the indicator on the surface of the catalyst, as a result of a contribution of all accessible acidic and basic sites in the catalyst. An indicator with a higher pK_a is deprotonated only upon reaction on stronger basic sites. When the amount of deprotonated molecules is higher than protonated molecules ($[A^-]>>[AH]$, (see Scheme 4 in Chapter 2.2.4), the basic color is observed. These deprotonated molecules can, however, react again with the acidic sites in the catalyst and thereby be transformed again into the protonated form. Thus, when the basic color of a specific indicator is observed, this indicates that the basic sites of the investigated catalyst have a higher pK_a than the indicator and that those basic sites are present in a higher amount than the acidic sites which are capable of reprotonating the basic indicator molecules.

Table 5 also shows the results for the color changes for four non-impregnated catalysts and for the single oxides, silica and magnesia. CP-MOD and the CuO-promoted catalysts posses an intrinsic coloration, thus color change of the indicator cannot be easily observed; therefore, these catalysts were left out during studies with Hammett indicators. The performed experiments show that a pK_a between 7.2 and 9.3 can be attributed to silica, given that the last indicator which shows the coloration due to the basic form is Bromothymolblue and the first one that does not change color is phenolphthalein (see Table 5); therefore silica is the most acidic sample of the samples tested. In comparison with pyridine-FTIR results, this is difficult to explain, as it was shown that silica contains the lowest amount of acidic sites. However, while performing Hammett indicator studies, the basic properties together with the acidic ones of the samples are involved, thus the results can be explained considering that silica is the least basic sample (presence of lowest concentration of basic

sites). As expected, magnesia is the most basic sample as its pK_a is between 18.4 (4-nitroaniline) and 26.5 (4-chloroaniline).

Table 5: Results for the Hammett indicators

	Bromothymolblue pK_a 7.2		Phenolphtalein pK_a 9.3		2,4-dinitroaniline pK_a 15.0		4-chloro-2-nitroaniline pK_a 17.2		4-nitroaniline pK_a 18.4		4-chloroaniline pK_a 25.5		Diphenylmethane pK_a 35	
A/B	*Yellow*	*Green*	*Colorless*	*Red*	*Yellow*	*Violet*	*Yellow*	*Orange*	*Colorless*	*Orange*	*Colorless*	*Pink*	*Colorless*	*Yellow/orange*
SiO$_2$	Color change		No color change											
MgO									Color change		No color change			
WK			Color change		Color change		No color change							
WK-MOD			Color change		Color change		No color change							
WK-AER			Color change		Unsure		No color change							
CP			Color change		No color change									
CP-MOD	-		-		-		-		-		-		-	

From what is reported in Table 5, it can be seen that the two most basic samples among the SiO$_2$-MgO catalysts, according to the Hammett indicators study, are WK and WK-MOD. Both have a bulk pK_a between 15.0 (2,4-dinitroaniline) and 17.2 (4-chloro-2-nitroaniline), thus a distinction between the two samples cannot be made with the use of the employed Hammett indicators. The CP catalyst is the least basic sample according to the results shown in Table 5. Its bulk pK_a value is between 9.3 (phenolphthalein) and 15.0 (2,4-dinitroaniline). The WK-AER has a bulk pK_a below 17.2 (2,4-dinitroaniline) and above 9.3 (phenolphthalein) but for this sample the color change could not be observed clearly when employing 2,4-dinitroaniline, having a pK_a value of 15.0. The suspension showed a yellow coloration, but this was observed to be significantly darker as compared with the initial color of the indicator solution. 2,4-dinitroaniline is yellow when in the acidic form and violet in the basic tone. Therefore, it is proposed that the bulk pK_a of the WK-AER catalyst is around 15.0, thus the acidic and basic form coexist originating a color which is a combination of colors of the two forms. Hammett indicator studies show the order in overall basicity for the tested catalysts to be: WK ≈ WK-MOD > WK-AER > CP.

The results from the experiments with the seven Hammett indicators are in accordance with the results for the catalytic performance (see Figure 2 in chapter 1.3.3). Figure 2 shows that CP is the catalyst which yields the highest amount of ethylene. This indicates that the catalyst has higher acidity as compared with the other silica-magnesia catalysts. The Hammett indicator method shows that the CP sample is the least basic, which can imply high acidity as well, which is expected from its catalytic performance. Catalytic results reported in Figure 2 show that the WK-AER catalyst leads to a lower ethylene production than CP, but higher than WK and WK-MOD; this was also confirmed by the results obtained from the Hammett indicator study, as shown in Table 5.

A point of discussion concerns the observed colors after the Hammett experiments. Often, it was difficult to determine both the possible color changes and the initial color of the solution. Color interpretation is a subjective parameter, thus it is difficult to interpret them objectively. However,

sometimes colors in between the given acidic and basic color were observed and occasionally even a completely different color was seen. For instance, the color of bromothymol blue is yellow in its acidic form and green in its basic form. The observed color, however, was purple. It was assumed that this color is associated with the deprotonated form, since it is a different color than the initial acidic color in solution (yellow). A possible explanation for this phenomenon is that due to the fact that there is a variety in strength for the acidic and basic sites, a part of the indicator molecules is not fully (de)protonated when reacting with acidic or basic sites in the catalyst. This means that there are not only indicator molecules in solution present, giving rise to a certain color, but also indicator molecules coordinated to active sites. These coordinated molecules can, in principle, give rise to different colors compared with the free molecules in solution.

4.2.2.2 Deuterated Chloroform-FTIR

Figure 17 reports the results for deuterated chloroform-FTIR; bands for adsorbed deuterated chloroform appear in the range 2000-2400 cm^{-1}.[71] For these experiments, deuterated chloroform (referred to herein as CDCl$_3$) is preferred to chloroform, since the C-H vibrations, unlike C-D vibrations, show absorption in the spectroscopic range where peaks due to O-H vibrations are observed as well.[71] The spectra shown in this thesis were all taken at a temperature of 50 °C, after 30 minutes since chloroform addition. After the experiments, it was often found that the infrared cell had assumed a dark coloration; this is explained by the formation of coke species due to chloroform reaction. In literature, it is reported that chloroform can react at elevated temperatures (i.e. higher than room temperature) on basic sites, thereby leading to formation of unwanted side-products.[61,78] The production of these undesired side-products possibly causes blocking of the basic sites, thus spectra taken at higher temperatures are considered not reliable. For this reason, spectra observed at a temperature higher than 50 °C in the TPD process are not shown in this thesis.

4.2.2.2.1 Silica-Magnesia Systems

Figure 17 shows the results for the CDCl$_3$-FTIR for four silica-magnesia catalysts and for magnesia. The CP-MOD catalyst was not analyzed with this method, as previously done for the Hammett indicator experiments.
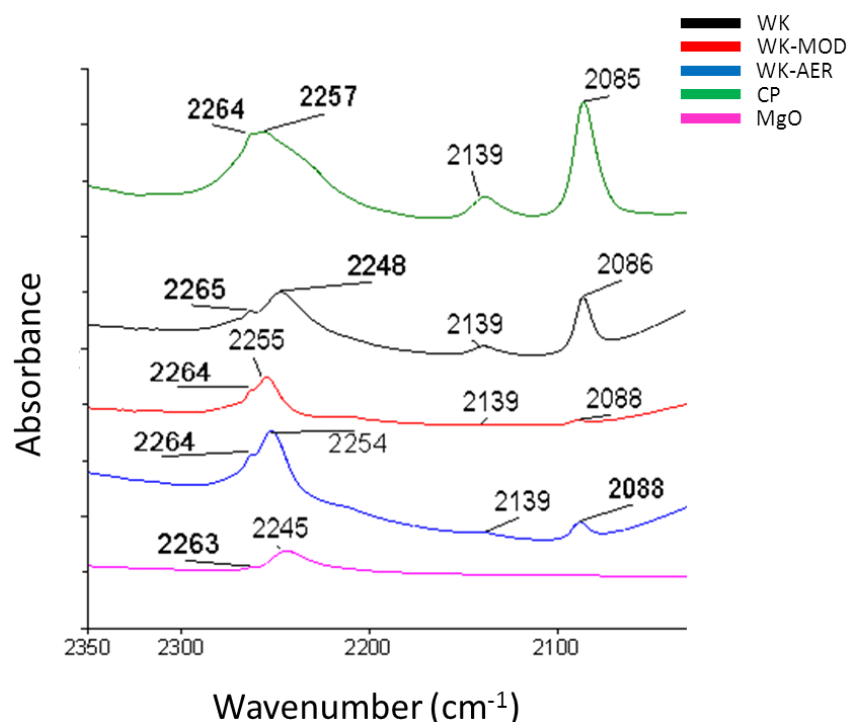

Figure 17: FTIR spectra at 50 °C showing the CDCl$_3$ region for the catalysts WK, WK-MOD, WK-AER, CP and for the single oxide MgO

The CDCl$_3$-FTIR spectrum for the studied samples shows the presence of two peaks. The low-intensity peak around 2263 cm^{-1} for magnesia is assigned to the C-D stretching of physisorbed deuterated chloroform; this band was also observed in the case of the four silica-magnesia catalysts studied. However, a band due to C-D stretching of deuterated chloroform adsorbed on silica is reported to have a similar position (around 2264 cm^{-1}).[71,78] Given that all catalysts contain silica, this assignment cannot be excluded for the silica-magnesia catalysts. The bands at approximately 2215 and 2250 cm^{-1} are assigned to chloroform chemisorbed on the basic sites of the catalyst under investigation. The presence of two different bands is due to the presence of, respectively, strong and weak basic sites.[61,71,78] A shift towards lower wavenumbers indicates the presence of stronger basic sites, as discussed in chapter 2.2.2.2.[74] Magnesia was observed to contain weak basic sites, showing a band at approximately 2245 cm^{-1}, assigned to C-D stretching of chemisorbed chloroform on weak basic sites. This is in contradiction with the results from the Hammett indicator study, which showed the presence of strong basic sites in magnesia. The four catalysts show this band, attributed to chloroform chemisorbed on weak basic sites at around 2250 cm^{-1}. As can be seen in Figure 17, the position of this band varies among the different catalysts, indicating a different strength of the basic sites. The band for the WK catalyst is observed at approximately 2248 cm^{-1} (lowest wavenumber as compared with the other catalysts). This means that the WK catalyst contains the strongest basic sites.[74] This result is also in accordance with the results from the Hammett indicator study. WK-MOD and WK-AER show the band due to C-D stretching of deuterated chloroform adsorbed on weak basic sites at similar position, while in the case of the CP catalyst it is shifted towards higher wavenumbers the most with respect to the C-D stretching band of chloroform adsorbed on magnesia. This indicates that the CP sample has the weakest basic sites, which complies with the results from the Hammett indicator study. The four catalysts under study also show a shoulder at approximately 2215 cm^{-1}, assigned to strong basic sites according to Paukshtis *et al*.[71] This shoulder was not observed to be present when investigating magnesia. Additionally, Figure 17 shows the peak located at approximately 2250 cm^{-1} to have lower intensity in the case of magnesia as compared with the silica-magnesia catalysts. This result is quite surprising as magnesia is expected to contain a quite high amount of basic sites, also based on what was observed in the case of the Hammett indicator study.[61] An explanation, related to the fact that CDCl$_3$ can become reactive at basic sites, is the possible blockage of the strong basic sites in magnesia due to reaction of chloroform on basic sites. Consequently, the band at approximately 2215 cm^{-1}, assigned to the C-D stretching of deuterated chloroform chemisorbed on strong basic sites, is not present for magnesia.

Furthermore, all four catalysts show two additional bands at around 2139 and 2086 cm^{-1}. The ratio for the intensities of the two peaks is different for each catalyst. These two peaks have not been reported in literature before, so their attribution can only be tentative. In section 4.4 of this thesis a hypothesis is proposed on the origin of these bands, in which the peaks are attributed to further weakened C-D vibrations due to interaction with a second basic site.

4.2.2.2.2 Influence of CuO

Three catalysts, doped with CuO (WK, WK-MOD and CP), were tested with deuterated chloroform-FTIR. CP and WK were tested, because, based on results from pyridine-FTIR, NH$_3$-TPD and the Hammett indicator study, they represent, respectively, the most acidic and most basic catalyst. WK-MOD was chosen due to its remarkable catalytic performance, as can be seen in Figure 2 in section 1.3.3.

Figure 18 shows the comparison between the spectra of the three studied catalysts with and without copper oxide at 50 °C in the chloroform C-D stretching region. CP seems to lose a quite significant amount of basic sites after doping the sample with CuO. The peaks at 2139 and 2085 cm^{-1} have completely disappeared and the intensity of the peaks at 2264 and 2256 cm^{-1} is considerably lower for the CuO-promoted catalyst. In the WK catalyst, the peaks at 2139 and 2085 cm^{-1} cannot be observed for the CuO-doped catalyst; furthermore, the peak at 2245 cm^{-1} seems to be shifted to higher wavenumbers, thus indicating the presence of weaker basic sites. The basic properties of WK-MOD do not appear to change significantly upon CuO-doping. The bands at 2139 and 2089 cm^{-1} are characterized by quite low intensity in the non-impregnated sample, thus not much can be said in the case of the impregnated one. The intensities of the bands at approximately 2264 and 2256 cm^{-1} are quite similar; however, the peak at 2256 cm^{-1} seems to be shifted to higher wavenumbers, similar to what was observed for CuO/WK.
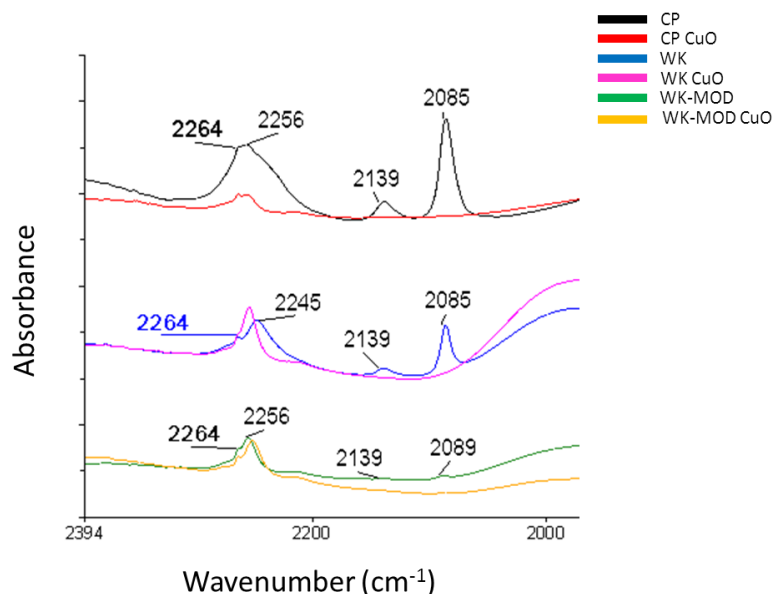

Figure 18: FTIR spectra at 50 °C showing the CDCl$_3$ region for the catalysts WK, WK-MOD and CP with and without CuO-promotion

4.3 Spatially-Resolved Characterization Techniques

Coherent Anti-Stokes Raman Scattering (CARS) microscopy was employed as a spatially-resolved characterization technique. In order to surpass the diffraction limit of the microscope, the catalyst WK-BIG, employing silica spheres of 1.8 µm, was synthesized. Section 4.3.1 describes the results for the synthesis of these large silica spheres and section 4.3.2 deals with the results of the CARS experiments.

4.3.1 Synthesis WK-BIG

A seed batch with silica spheres was prepared to employ in a consecutive growth step. The TEM micrograph for the yielded silica in this seed batch having a spherical morphology can be seen in Figure 6. The preparation of the seed batch yielded silica spheres, which were quite monodisperse, with an average diameter of 900 nm.
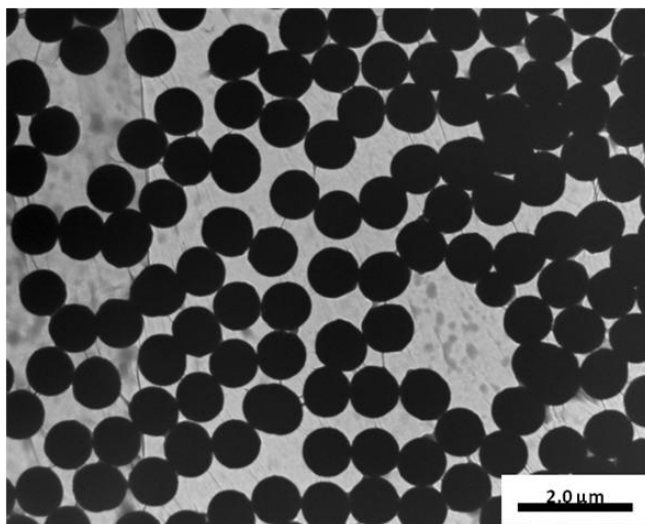
Figure 19: TEM micrographs the seed batch, average particle size 900 nm

The 900 nm batch was used for the consecutive growth step with the aim to achieve particle sizes as large as possible. During the growth step, TEOS, ammonia, ethanol and water were added in a continuous way; this procedure resulted in average particle sizes of 1.8 µm (see Figure 20). It can be observed that a second nucleation had taken place, which is indicated by the presence of significantly smaller particles. Silica obtained as described was then used for wet-kneading with magnesium hydroxide to prepare catalyst WK-BIG; this silica-magnesia material was analyzed with CARS.

Figure 20: TEM micrographs after the growth process. Average particle size 1.8 µm

4.3.2 Coherent Anti-Stokes Raman Scattering (CARS) Micro-Spectroscopy

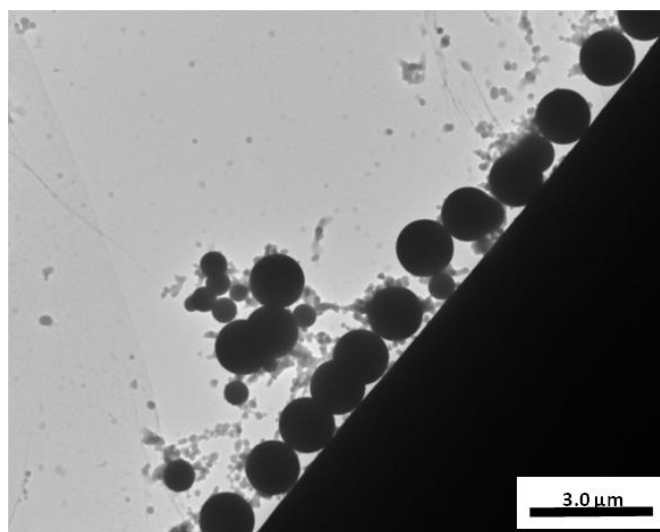WK-BIG was analyzed with CARS to locate pyridine adsorbed on the catalyst by detecting its Raman signal. In particular, the goal was the localization of the acidic sites in the silica- or magnesia-rich region, due to the adsorption of the basic probe molecule pyridine. The resolution of the microscope was around 300 nm per pixel. Therefore, WK-BIG, employing silica spheres with a diameter of 1.8 micron, was tested.

Unfortunately, CARS analysis did not lead to the desired results for two reasons: first, it was difficult to distinguish Raman signal of silica in the catalyst from silica present in the glass slide and cover slip employed to perform the experiment. More importantly, the Raman signal of pyridine could not be observed for the sample studied. Similar experiments were successfully performed on zeolites[97]; this might be due to the fact that pyridine molecules are confined in the small pores of zeolites, thus leading to a significantly enhanced Raman signal.

Alternative spatially-resolved spectroscopic methods, such as UV-VIS microscopy or confocal fluorescence microscopy did not lead to positive results, due to the fact that the optical light microscopes used in these methods do not possess the resolutions required to distinguish the silica spheres and magnesia platelets present in the catalyst.

4.4 Discussion

Acidity Study

The acidity study showed that the CP catalyst contained the highest amount of acidic sites and the strongest acidic sites, which is in line with the catalytic results shown in Figure 2. During catalytic reaction, ethylene is produced when ethanol reacts at acidic sites, therefore it was postulated that a high production of ethylene indicates a high amount of acidic sites. The product distribution for the CP catalyst indeed shows the highest production of ethylene compared with the other silica-magnesia catalysts, which, therefore, supports this direct relation between acidity and ethylene production. However, results for the acidity study of the WK-AER catalyst show some inconsistencies. Although both methods showed that CuO/WK-AER contains the highest concentration of acidic sites compared with other CuO-promoted silica-magnesia catalysts, NH_3-TPD showed a significant increase in the concentration of acidic sites upon CuO-promotion, while pyridine-FTIR showed a decrease. Zaccheria *et al.* investigated the influence of CuO nanoparticles dispersed on silica spheres on the amount of acidic sites and they found that a high dispersion of CuO particles induced acidic behavior, which could be ascribed to the coordinative unsaturation of the very small nanoparticles. This unsaturation makes the CuO particles prone to coordinate surrounding molecules.[92] The results shown by Zaccheria *et al.* are in line with the observed increase in acidity for WK-AER upon CuO-promotion. However, it also immediately raises the question on why this increase was only observed for the WK-AER and, moreover, why this increase was not observed in pyridine-FTIR results. It is possible that part of the acidic sites present in the catalysts are only accessible for small molecules, such as ammonia. This indicates that larger probe molecules, such as pyridine, cannot reach the acidic sites. Thus, it can be postulated that upon CuO-promotion, in some catalysts the acidic sites become less accessible due to pore blockage of CuO particles. This hypothesis also explains the inconsistency between results from NH_3-TPD and pyridine-FTIR for the WK catalyst. NH_3-TPD showed only a small decrease for the amount of acidic sites present in WK upon CuO-promotion, whereas pyridine-FTIR showed no peaks, attributed to pyridine coordinated to acidic sites, anymore for CuO/WK. Apparently, upon CuO-promotion, the acidic sites are only accessible for small molecules such as ammonia. The question regarding why the observed increase in concentration of acidic sites for the CuO/WK-AER was not observed for the other catalysts, probably concerns the differences in morphology between the catalysts. WK-AER contains small silica spheres (20-40 nm) embedded in magnesia layers, which might result into better accessibility for the active sites compared with the wet-kneaded catalysts employing larger silica spheres. The CP catalyst showed a large significant

decrease in concentration of acidic sites, which, in this perspective, might indicate that CuO causes a large decrease in porosity, resulting into badly accessible active sites. The influence of CuO on possible blockage of active sites requires further investigation.

Section 4.2.1.1.1 showed that the peak at 3670 cm^{-1} in the IR spectrum of a dried catalyst was assigned to an O-H vibration, in which the hydroxyl group has interaction with both silicon and magnesium atoms. This assignment was based on the IR spectrum of Antigorite, a mineral with the molecular formula $Mg_3Si_2O_5(OH)_4$, which showed only one sharp peak at 3670 cm^{-1} in the OH region.[89] The trend in which the wet-kneaded catalysts showed an increase in intensity for the peak at 3670 cm^{-1} with decreasing silica sphere size is in line with this assignment, as smaller silica spheres possess larger surface areas per gram and thus have more interaction with the magnesia. However, the CP catalyst only showed a large peak at 3730 cm^{-1}, attributed to the OH vibration found in brucite $Mg(OH)_2$ or basic OH groups.[70] This result was unexpected, since the CP catalyst, prepared via co-precipitation of TEOS and $Mg(NO_3)_2$, is expected to have many interactions between silicon, magnesium and oxygen atoms. Moreover, Iishi *et al.* reported a synthesis for the mineral Antigorite, which is quite similar to the preparation method used in this thesis for the CP catalyst. They prepared Antigorite by dispending ethanolic solutions of tetraethyl orthosilicate and magnesium nitrate, followed by hydrolyzation by addition of NH_4OH and drying of the precipitate.[98] This synthesis is quite similar to the co-precipitation method as described in section 2.1.4. Therefore, it is expected that Antigorite and CP exist of similar structures, leading to similar peak positions in the IR spectrum. Kermarec *et al.* observed two different bands due to hydroxyl groups in silica-magnesia systems, prepared from a sol-gel solution, at 3710 and 3670 cm^{-1}. They assigned the band at 3670 cm^{-1} to the presence of OH bonded to tetra-coordinated magnesium and the band at 3710 cm^{-1} to octahedrally coordinated magnesium.[60] Therefore, it is suggested that although Antigorite and CP are prepared via similar synthesis methods, CP contains hydroxyl groups bound to magnesium atoms with octahedral coordination, leading to a peak at 3730 cm-1 and Antigorite contains hydroxyl groups bound to magnesium with lower coordination numbers. This hypothesis is supported by the XRD results reported by Dungan *et al.*, who showed that octahedral occupancy of the atoms is low in Antigorite.[99] To the best of our knowledge, there is no literature concerning the atomic arrangements in Antigorite, therefore it would be interesting to study the structural differences between Antigorite and CP in order to test the proposed hypothesis as described above.

Basicity Study

Deuterated chloroform-FTIR measurements showed that magnesia only contained weak basic sites, which is unexpected, since it is known from literature that magnesia contains strong basic sites.[100] Moreover, Hammett indicators showed that magnesia contains the strongest basic sites, compared with silica-magnesia catalysts. These two inconsistencies suggest that the results from deuterated chloroform-FTIR are not reliable. It is known from literature that deuterated chloroform can become reactive on basic sites at elevated temperatures.[61,78] Therefore, it is proposed that at strong basic sites deuterated chloroform becomes already reactive at 50 °C, which is the temperature at which deuterated chloroform was applied to the samples. During this reaction of deuterated chloroform on basic sites, coke-like species might be formed, which block the strong basic sites in magnesia. This hypothesis is confirmed by the fact that after $CDCl_3$-FTIR measurements, the cell, containing the sample holder, was often contaminated with thick layers of black/brown/orange coke-like species. Therefore, it might be interesting to apply the deuterated chloroform on magnesia at room temperature in order to verify the presence of strong basic sites. Moreover, measurements at room temperatures could also verify if the shoulders observed for the different silica-magnesia catalysts at 2215 cm^{-1} could indeed be attributed to deuterated chloroform adsorbed on stronger basic sites.

Furthermore, all four catalysts showed bands at around 2139 and 2086 cm^{-1}. These two peaks have not been reported in literature before, so their attribution can only be tentative. As mentioned, the bands located at around 2250 and 2215 cm^{-1} are originating from the C-D stretching of chemisorbed deuterated chloroform. When CDCl$_3$ chemisorbs on a basic site, the deuterium is partially attracted by the basic site, thus the C-D bond is weaker than in physisorbed chloroform; this causes lowering in the wavenumber of the considered vibration (from 2263 cm^{-1} for physisorbed CDCl$_3$ to 2250 and 2215 cm^{-1} for CDCl$_3$ chemisorbed on weak and strong basic sites, respectively). The two bands at approximately 2139 and 2086 cm^{-1} are proposed to be additional C-D vibrations, in which the C-D bond has been further weakened. In particular, it is possible that a basic site interacts with the deuterium and an additional closely located second basic site interacts with the electropositive carbon atom in chloroform, as can be seen in Figure 21. Both interactions involve the donation of electrons into the C-D bond, causing additional weakening. This combined interaction between the deuterated chloroform and two closely located basic sites weakens the C-D stretching vibration even more, thus originating the additional bands observed in Figure 17. As can be seen in Figure 18, these additional bands disappear upon CuO-promotion and for some catalysts the amount of basic sites decreases. A possible explanation for this observation is that CuO particles, anchored on the surface hydroxyl groups, decrease accessibility of basic sites, similar to its effect on the acidic sites as described above. Thus, this is a second indication that CuO-promotion induces structural changes, leading to a decrease in accessibility of active sites.
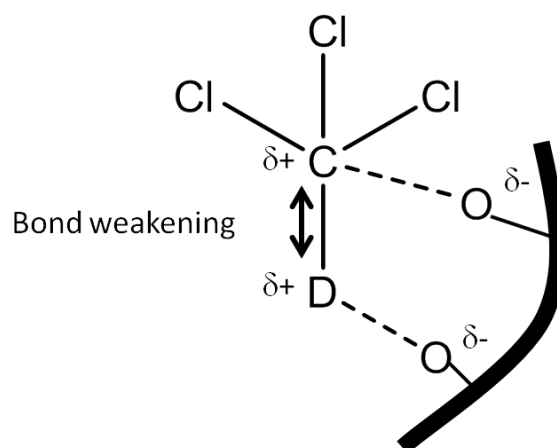

Figure 21: The proposed structure of deuterated chloroform interacting with two basic sites, thereby weakening the C-D vibration

Chapter 5. Conclusion

The acidic and basic properties of the silica-magnesia catalysts strongly depend on the catalyst preparation method. Different hydroxyl groups are observed during IR study for the catalysts and their abundance and nature vary significantly for samples prepared with different procedures. Only when both silica and magnesia are present, a peak characterized by absorption at approximately 3670 cm^{-1} is observed; this is assigned to hydroxyl groups bonded to magnesium and silicon as reported for the mineral Antigorite.

NH$_3$-TPD and pyridine-FTIR show that the CP catalyst contains the highest amount of acidic sites and that the WK catalyst contains the lowest amount. The order in amount of acidic sites for the different silica-magnesia catalysts is CP > WK-AER > WK-MOD > WK. This accounts for both the concentration of acidic sites and the strength. The results for the acidic properties of the CP-MOD catalyst from the NH$_3$-TPD and the pyridine-FTIR are not completely in accordance. The catalysts only contain Lewis acidity, which is proposed to be originated from the magnesia and from the interaction between magnesia and silica.

CuO is anchored to hydroxyl groups on the surface of the catalysts. This is indicated by the decrease in intensity of the peaks due to OH absorption upon CuO-promotion for all samples. Furthermore, upon CuO-doping, the strength and concentration of the acidic sites in the co-precipitated samples are decreased significantly. The influence of the CuO on the acidic properties of the wet-kneaded samples differs considerably when comparing the catalysts. The strength of acidic sites in the WK-MOD and the WK-AER catalysts increases due to CuO, according to the pyridine-FTIR results. NH$_3$-TPD shows that the concentration of acidic sites decreases in the case of WK-MOD, similar to the co-precipitated catalysts, whereas it increases in the WK-AER. The results for the WK catalyst are more difficult to interpret. Pyridine-FTIR shows that WK loses most of its acidic sites upon CuO-doping, while the TPD results show that the acidic properties do not change significantly. It is possible that the accessibility of the acidic sites change due to the CuO, since ammonia molecules are smaller than pyridine.

Chloroform-FTIR and the Hammett indicator experiments both confirm that the WK catalyst contains the strongest basic sites and the CP catalyst the weakest. The order in strength of the basic sites for the catalysts is WK > WK-MOD > WK-AER > CP. Due to uncertainty in the assignment of the peaks at 2139 and 2086 cm^{-1} and due to possible basic site blockage by coke-like species, caused by reactive deuterated chloroform at basic sites, it is not possible to confirm the results from the Hammett indicators with the chloroform-FTIR. Therefore, further studies might be useful to shed light on the basic properties of the catalysts.

The influence of CuO on the basic properties of the catalysts was tested with deuterated chloroform-FTIR for three selected catalysts. The concentration of basic sites decreases significantly in the CP catalyst upon CuO doping, similar to the influence on the acidic properties. The spectra for the WK-MOD catalyst do not show considerable changes in the basic properties due to the presence of CuO. The spectrum for the CuO/WK catalyst does not show bands around 2139 and 2085 cm^{-1} and indicates a change in strength of the basic sites.

Chapter 6. Recommendations

In this section, a few suggestions for research are recommended in order to confirm the results reported in this thesis and to overcome the inconsistencies observed. First of all, the synthesis of the CP-MOD catalyst suffered from some still unresolved problems. Unlike the other silica-magnesia catalysts, the CP-MOD is not white, but shows a darker coloration. This made it impossible to use the catalyst in the Hammett indicator experiments. Also, the results for the acidic properties of the CP-MOD catalyst were not consistent. Therefore, it is recommended to optimize the synthesis conditions for the CP-MOD, which would hopefully lead to more consistent results. Secondly, the conditions for the experiments with the deuterated chloroform-FTIR setup need to be optimized. Further research must be done in order to get more insight in possible unwanted reactions suffered by chloroform at elevated temperatures. In case these problems cannot be solved, the possibility of using alternative probe molecules for basicity should be taken into account. Furthermore, $CDCl_3$-FTIR results show a relatively low concentration of weak basic sites for magnesia, which was unexpected. Further research is required to explore the nature and strength of basic sites in magnesia. A possibility would be to perform CO_2-TPD measurements. Also, the influence of CuO-promotion on the acidic properties of the catalysts were studied extensively. To get more insight on the effects of CuO, it would be interesting to perform a more extensive complementary study, investigating the influence of CuO-doping on the basic properties.

In this thesis, the acidic and basic properties of the catalysts were mainly studied with the use of bulk characterization techniques. The use of spatially-resolved characterization techniques could shed more light on the different product distributions after catalytic reaction when comparing the silica-magnesia(-copper oxide) catalysts. The attempts to work with spatially-resolved techniques did not lead to desired results. The low resolutions in light microscopes did not allow to distinguish the magnesia- and silica-rich regions present in the different catalysts; thus alternative techniques employing high-resolution microscopes, such as an electron microscope, should be employed. It is recommended to perform an EELS (Electron Energy Loss Spectroscopy) study combined with cryo-TEM on pyridine-probed silica-magnesia systems. The combination of the two methods allows to spatially resolve the location of the chemisorbed pyridine. Cryo-TEM is performed to prevent the pyridine from evaporation in the electron beam. Furthermore, more research concerning structural differences between the catalysts, related to the differences in acidic and basic properties, is required. In particular, section 4.4 discusses the influence of CuO-promotion on the acidic and basic properties and it is proposed to further investigate the influence of CuO particles on structural changes, leading to different accessibility of active sites.

Chapter 7. Acknowledgements

First of all, I like to thank Pieter and Bert for giving me the opportunity to do my master thesis in this group. Pieter, thank you for the many meetings we had, for your time and for many great and interesting ideas and suggestions for my project. Your enthusiasm increased my interest in research even more. Bert, we never spoke about the content of my project, but I like to thank you for your overall interest in me as a student. You regularly walked by to inform if everything was ok, which was appreciated. Also, you made it possible for me to finish my master with a half year project at Stanford University, which is a dream come true for me, so thank you.

Carlo, we have worked on this project together for almost 1.5 years. For my master thesis I wanted a project involving many different techniques, to learn as much as possible. You gave me a very interesting project with many analytical techniques. Even though not every method was successful for our project, I have had the opportunity to learn about the fundamentals and principles of every technique, which was absolutely interesting. I also want to thank you for being a great mentor for me. I felt that I could always talk to you if I had any questions, you were always prepared to make time for me. You taught me a lot when it comes to work in the lab, I admire the way you work so precise, clean and tidy. I will always keep that in mind when working in the lab. At the end of this project, I am proud of the results we achieved together. I look forward to hearing about your further results and wish you the best in your last years of PhD research.

Fouad, your help with the IR spectroscopy was absolutely useful. Thank you for your help with the setup and with the interpretation of the data. Also, we have had many both interesting and fun conversations in the IR room and at our desks.

Ramon, is acknowledged for measuring my samples on the TPD. Hendrik, Qingyun, Ad Mens and Ad van Eerden are acknowledged for their help with the pyridine FTIR and for helping me to build the chloroform IR setup. Sophie, thank you for giving up your time on the pyridine-FTIR to let me do my last measurements. Joe, thank you for teaching me how to work with the Hammett indicators. Joe and Fiona are both acknowledged for letting me use their fumehood many times and for their help with the schlenk lines.

Judith Wijnhoven is acknowledged for her help with the synthesis of large silica particles at the Soft Condensed Matter group. Hans Meeldijk is acknowledged for his help with the TEM microscope and our attempts to do EELS. You are a good teacher and your explanations were very clear to me.

I like to thank the entire biomass group for their useful suggestions for my research during our very interesting, yet long and exhausting meetings.

And last, I want to thank Katinka and Wuliyasu for being my friends and giving me support at our desks.

Chapter 8. References

[1]   P. E. Hodgson, *Modern Age*, vol. 50, no. 3, 2008.

[2]   www.epa.gov/climatechange, *EPA, United States Environmental Protection Agency*. .

[3]   C. Angelici, B. M. Weckhuysen, and P. C. a Bruijnincx, *ChemSusChem*, vol. 6, pp. 1–21, May 2013.

[4]   A. Corma, S. Iborra, and A. Velty, *Chemical reviews*, vol. 107, no. 6, pp. 2411–502, Jun. 2007.

[5]   P. Gallezot, *ChemSusChem*, vol. 1, no. 8–9, pp. 734–7, Jan. 2008.

[6]   www.biomassenergycentre.org.uk.

[7]   J. Zakzeski, P. C. a Bruijnincx, A. L. Jongerius, and B. M. Weckhuysen, *Chemical reviews*, vol. 110, no. 6, pp. 3552–99, Jun. 2010.

[8]   J. J. Bozell and G. R. Petersen, *Green Chemistry*, vol. 12, no. 4, p. 539, 2010.

[9]   J. Van Haveren, E. L. Scott, and J. Sanders, *Biofuels, Bioproducts and Biorefining*, vol. 2, pp. 41–57, 2008.

[10]   J. Lian, S. Chen, S. Zhou, Z. Wang, J. O'Fallon, C.-Z. Li, and M. Garcia-Perez, *Bioresource technology*, vol. 101, no. 24, pp. 9688–99, Dec. 2010.

[11]   J. Szczodrak and J. Fiedurek, *Biomass and Bioenergy*, vol. 10, no. 5–6, pp. 367–375, Jan. 1996.

[12]   P. C. Badger, "Ethanol From Cellulose : A General Review," in *Trends in new crops and new uses*, J. Jandick and A. Whipkey, Eds. Alexandria, VA, 2002, pp. 17–21.

[13]   W. C. White, *Chemico-biological interactions*, vol. 166, no. 1–3, pp. 10–4, Mar. 2007.

[14]   C. N. Hamelinck, G. Van Hooijdonk, and A. P. Faaij, *Biomass and Bioenergy*, vol. 28, no. 4, pp. 384–410, Apr. 2005.

[15]   OECD/FAO, "OECD-FAO Agricultural Outlook 2011-2020.

[16]   A. D. Patel, K. Meesters, H. den Uil, E. de Jong, K. Blok, and M. K. Patel, *Energy & Environmental Science*, vol. 5, no. 9, p. 8430, 2012.

[17]   B. Tait, *FSSA J.*, pp. 27–28, 2005.

[18]   L. Wu, Y. Li, M. Arakane, M. Ike, M. Wada, Y. Terajima, S. Ishikawa, and K. Tokuyasu, *Bioresource technology*, vol. 102, no. 24, pp. 11183–8, Dec. 2011.

[19]   M. M. Kücük and A. Demirbas, *Energy Conversion Management*, vol. 38, pp. 151–165, 1997.

[20]   S. González-García, L. Luo, M. T. Moreira, G. Feijoo, and G. Huppes, *Biomass and Bioenergy*, vol. 36, pp. 268–279, Jan. 2012.

References

[21]   D. Pimentel and T. W. Patzek, *Natural Resources Research*, vol. 14, no. 1, pp. 65–76, Mar. 2005.

[22]   C. S. Goh and K. T. Lee, *Renewable and Sustainable Energy Reviews*, vol. 14, no. 2, pp. 842–848, Feb. 2010.

[23]   R. P. John, G. S. Anisha, K. M. Nampoothiri, and A. Pandey, *Bioresource technology*, vol. 102, no. 1, pp. 186–93, Jan. 2011.

[24]   N. L. Morrow, *Environmental Health Perspectives*, vol. 86, pp. 7–8, 1990.

[25]   J. Ostromislenskiy, *Journal of Russian Physical-Chemical Society*, vol. 47, p. 1472, Jun. 1915.

[26]   S. W. Lebedev, *British Patent*, vol. 331, no. 402, May 1929.

[27]   S. W. Lebedev, *Russian Journal of General Chemistry*, vol. 3, pp. 698–708, May 1933.

[28]   S. W. Lebedev, *Chemiker-Zeitung*, vol. 60, pp. 313–316, May 1936.

[29]   E. V. Makshina, W. Janssens, B. F. Sels, and P. a. Jacobs, *Catalysis Today*, vol. 198, pp. 338–344, Jun. 2012.

[30]   W. M. Quattlebaum, W. J. Toussaint, and J. T. Dunn, *Journal of the American Chemical Society*, vol. 69, pp. 593–599, 1947.

[31]   V. Gruver, A. Sun, and J. J. Fripiat, *Catalysis Letters*, vol. 34, no. 3–4, pp. 359–364, 1995.

[32]   G. Natta and R. Rigamonti, *Chimica e l'Industria*, vol. 29, pp. 195–201, 1947.

[33]   G. Natta and R. Rigamonti, *Chimica e l'Industria*, vol. 29, pp. 3–8, 1947.

[34]   H. Niiyama, S. Morii, and E. Echigoya, *Bulletin of the chemical society of Japan*, vol. 45, pp. 655–659, 1972.

[35]   R. Ohnishi and K. Tanabeb, *Chemistry Communications*, vol. 70, pp. 1613–1614, 1985.

[36]   S. Kvisle, A. Aguero, and R. P. a. Sneeden, *Applied Catalysis*, vol. 43, no. 1, pp. 117–131, Jan. 1988.

[37]   M. D. Jones, C. G. Keir, C. Di Iulio, R. a. M. Robertson, C. V. Williams, and D. C. Apperley, *Catalysis Science & Technology*, vol. 1, no. 2, p. 267, 2011.

[38]   W. Stöber and A. Fink, *Journal of Colloid and Interface Science*, vol. 26, no. 1, pp. 62–69, 1968.

[39]   R. Brambilla, C. Radtke, J. H. Z. dos Santos, and M. S. L. Miranda, *Powder Technology*, vol. 198, no. 3, pp. 337–346, Mar. 2010.

[40]   U. University, "1st years Chemistry UU prescription: De bereiding van silica en de verestering van zijn oppervlak met stearyl alcohol." 1997.

[41]   H. Giesche, *Journal of the European Ceramic Society*, vol. 14, no. 3, pp. 189–204, Jan. 1994.

References

[42]   J. Haber, J. H. Block, and B. Delmon, *Pure and Applied Chemistry*, vol. 67, no. 8/9, pp. 1257–1306, 1995.

[43]   H. Giesche, *Journal of the European Ceramic Society*, vol. 14, no. 3, pp. 205–214, Jan. 1994.

[44]   PCT/US90/03605.

[45]   US Patent 4,911,930.

[46]   M. Wolters, P. Munnik, J. H. Bitter, P. E. de Jongh, and K. P. de Jong, *The Journal of Physical Chemistry C*, vol. 115, no. 8, pp. 3332–3339, Mar. 2011.

[47]   W. M. Tolles, J. W. Nibler, J. R. Mcdonald, and A. B. Harvey, *Applied Spectroscopy*, vol. 31, no. 4, pp. 253–271, 1977.

[48]   J. Cheng and X. S. Xie, *Journal of Physical Chemistry B*, vol. 108, pp. 827–840, 2004.

[49]   A. Zumbusch, G. Holtom, and X. Xie, *Physical Review Letters*, vol. 82, no. 20, pp. 4142–4145, May 1999.

[50]   C. L. Evans, E. O. Potma, M. Puoris'haag, D. Côté, C. P. Lin, and X. S. Xie, *Proceedings of the National Academy of Sciences of the United States of America*, vol. 102, no. 46, pp. 16807–12, Nov. 2005.

[51]   C. L. Evans and X. S. Xie, *Annual review of analytical chemistry (Palo Alto, Calif.)*, vol. 1, pp. 883–909, Jan. 2008.

[52]   M. Müller and A. Zumbusch, *Chemphyschem : a European journal of chemical physics and physical chemistry*, vol. 8, no. 15, pp. 2156–70, Oct. 2007.

[53]   W. M. Tolles and R. D. Turner, *Applied Spectroscopy*, vol. 31, no. 2, pp. 96–103, 1977.

[54]   W. Min, S. Lu, G. R. Holtom, and X. S. Xie, *Chemphyschem : a European journal of chemical physics and physical chemistry*, vol. 10, no. 2, pp. 344–7, Feb. 2009.

[55]   B. Schrader, *Infrared and Raman Spectroscopy*. London, UK: John Wiley and Sons, 1995.

[56]   R. L. Richardson and S. W. Benson, *Journal of Physical Chemistry*, vol. 61, no. 4, pp. 405–411, 1957.

[57]   A. Travert, A. Vimont, A. Sahibed-Dine, M. Daturi, and J.-C. Lavalley, *Applied Catalysis A: General*, vol. 307, no. 1, pp. 98–107, Jun. 2006.

[58]   M. Akçay, *Applied Catalysis A: General*, vol. 294, no. 2, pp. 156–160, Oct. 2005.

[59]   M. I. Zaki, M. A. Hasan, and F. A. Al-sagheer, *Colloids and Surfaces*, vol. 190, pp. 261–274, 2001.

[60]   M. Kermarec, M. Briend-Faure, and D. Delafosse, *Journal of the Chemical Society, Faraday Transactions 1*, vol. 70, p. 2180, 1974.

References

[61]   J. C. Lavalley, *Catalysis Today*, vol. 27, no. 3–4, pp. 377–401, Feb. 1996.

[62]   J. I. Di Cosimo, V. K. Díez, M. Xu, E. Iglesia, and C. R. Aperteguía, *Journal of Catalysis*, vol. 178, pp. 499–510, 1998.

[63]   V. Cedex, *Catalysis Letters*, vol. 40, pp. 249–252, 1996.

[64]   K. Sadowska, K. Góra-Marek, and J. Datka, *Vibrational Spectroscopy*, vol. 63, pp. 418–425, Nov. 2012.

[65]   E. P. Parry, *Journal of Catalysis*, vol. 2, pp. 371–379, 1963.

[66]   R. B. Borade, A. Adnot, and S. Kaliaguine, *Zeolites*, vol. 11, pp. 710–719, 1991.

[67]   A. Corma, C. Corell, W. Kolodziejski, J. Prez-pariente, I. D. T. Quimica, U. Polit, and D. Valencia, *Zeolites*, vol. 15, pp. 576–582, 1995.

[68]   A. Chambellan, T. Chevreau, S. Khabtou, M. Marzin, J. C. Lavalley, and U. R. A. Cnrs, *Zeolites*, vol. 12, pp. 306–314, 1992.

[69]   N. Echoufi and P. Gélin, *Catalysis Letters*, vol. 40, pp. 249–252, 1996.

[70]   D. R. M. Brew and F. P. Glasser, *Cement and Concrete Research*, vol. 35, no. 1, pp. 85–98, Jan. 2005.

[71]   E. A. Paukshtis, N. S. Kotsarenko, and L. G. Karakchiev, *Reaction Kinetics and Catalysis Letters*, vol. 12, no. 3, pp. 315–319, 1979.

[72]   J. Xie, M. Huang, and S. Kaliaguine, *Reaction Kinetics and Catalysis Letters*, vol. 58, no. 2, pp. 217–227, 1996.

[73]   M. Sa, T. Blasco, A. Corma, U. Rey, and J. Carlos, *Journal of Physical Chemistry C*, vol. 112, pp. 16961–16967, 2008.

[74]   M. Kustov, L, *Topics in Catalysis*, vol. 4, pp. 131–144, 1997.

[75]   M. Sánchez-Sánchez and T. Blasco, *Catalysis Today*, vol. 143, no. 3–4, pp. 293–301, May 2009.

[76]   D. P. Debecker, E. M. Gaigneaux, and G. Busca, *Chemistry (Weinheim an der Bergstrasse, Germany)*, vol. 15, no. 16, pp. 3920–35, Jan. 2009.

[77]   F. Winter, X. Xia, B. P. C. Hereijgers, J. H. Bitter, a J. van Dillen, M. Muhler, and K. P. de Jong, *The journal of physical chemistry. B*, vol. 110, no. 18, pp. 9211–8, May 2006.

[78]   Y. et al Ono, "Characterization of Solid Base Catalysts Methods of Characterization," in *Solid Base Catalysis*, 2011, pp. 11–68.

[79]   G. Tonetto, J. Atias, and H. de Lasa, *Applied Catalysis A: General*, vol. 270, no. 1–2, pp. 9–25, Aug. 2004.

References

[80]   S. Sugunan and A. Paul, *Indian Journal of Chemistry*, vol. 36, no. December, pp. 1068–1072, 1997.

[81]   J.-I. Take, N. Kikuchi, and Y. Yoneda, *Journal of Catalysis*, vol. 21, pp. 164–170, 1971.

[82]   L. P. Hammett and A. Deyrup, Columbia University, 1932.

[83]   C. H. Rochester, Chapter 7 in *Acidity Functions*, Academic Press, 1970, p. 234.

[84]   K. Tanabe, Chapter 3 in *Soid Acids and Bases*, Kodansha/Academic Press, 1970, p. 35.

[85]   L. Y. Shi, Y. M. Wang, A. Ji, L. Gao, and Y. Wang, *Journal of Materials Chemistry*, vol. 15, no. 13, p. 1392, 2005.

[86]   T. Tittabut and W. Trakarnpruk, *Industrial & Engineering Chemistry Research*, vol. 47, no. 7, pp. 2176–2181, Apr. 2008.

[87]   K. Tanabe and T. Yamaguchi, *Journal of the Research Institute for Catalysis*, vol. 02, pp. 179–184, 1964.

[88]   T. W. Dijkstra, R. Duchateau, R. a Van Santen, A. Meetsma, and G. P. a Yap, *Journal of the American Chemical Society*, vol. 124, no. 33, pp. 9856–9864, Aug. 2002.

[89]   www.rruff.info.

[90]   T. López, R. Gomez, M. E. Llanos, and E. López-Salinas, *Materials Letters*, vol. 38, pp. 283–288, 1999.

[91]   C. Angelici, B. M. Weckhuysen, and P. C. A. Bruijnincx, *submitted*.

[92]   F. Zaccheria, N. Scotti, M. Marelli, R. Psaro, and N. Ravasio, *Dalton transactions*, vol. 42, no. 5, pp. 1319–1328, Feb. 2013.

[93]   S. O. Marta León, Eva Díaz∗, *Catalysis Today*, vol. 164, pp. 436–442, 2011.

[94]   A. S. M. Junaid, M. Rahman, H. Yin, W. C. McCaffrey, and S. M. Kuznicki, *Microporous and Mesoporous Materials*, vol. 144, no. 1–3, pp. 148–157, Oct. 2011.

[95]   L. Rodríguez-González, F. Hermes, M. Bertmer, E. Rodríguez-Castellón, A. Jiménez-López, and U. Simon, *Applied Catalysis A: General*, vol. 328, no. 2, pp. 174–182, Sep. 2007.

[96]   I. L. C. Buurmans, J. Ruiz-Martínez, S. L. van Leeuwen, D. van der Beek, J. a Bergwerff, W. V Knowles, E. T. C. Vogt, and B. M. Weckhuysen, *Chemistry (Weinheim an der Bergstrasse, Germany)*, vol. 18, no. 4, pp. 1094–101, Jan. 2012.

[97]   E. G. Derouane, J. C. Védrine, R. R. Pinto, P. M. Borges, L. Costa, M. a. N. D. a. Lemos, F. Lemos, and F. R. Ribeiro, "*Catalysis Reviews: Science and Engineering*, vol. 55, no. 4, pp. 454–515, Oct. 2013.

[98]   K. Iishi, *American Mineralogist*, vol. 58, pp. 915–919, 1973.

References

[99]   M. A. Dungan, *Canadian Mineralogist*, vol. 17, pp. 771–784, 1979.

[100]   H. Gorzawski and W. Hoelderich, *Journal of Molecular Catalysis A: Chemical*, vol. 144, no. 1, pp. 181–187, Jul. 1999.